A STUDY ON NiTiSn LOW-TEMPERATURE SHAPE MEMORY ALLOYS AND THE PROCESSING OF NiTiHf HIGH-TEMPERATURE SHAPE MEMORY ALLOYS

Avery W. Young

Thesis Prepared for the Degree of

MASTER OF SCIENCE

UNIVERSITY OF NORTH TEXAS

May 2018

APPROVED:

Marcus L. Young, Major Professor
Sundeep Mukherjee, Committee Member
Jincheng Du, Committee Member
Othmane Benafan, Committee Member
Andrey Voevodin, Chair of the Department of Materials Science and Engineering
Costas Tsatsoulis, Dean of the College of Engineering
Victor Prybutok, Dean of the Toulouse Graduate School

Young, Avery W. *A Study on NiTiSn Low-Temperature Shape Memory Alloys and the Processing of NTiHf High-Temperature Shape Memory Alloys*. Master of Science (Materials Science and Engineering), May 2018, 68 pp., 2 tables, 24 figures, 289 numbered references.

Shape memory alloys (SMAs) operating as solid-state actuators pose economic and environmental benefits to the aerospace industry due to their lightweight, compact design, which provides potential for reducing fuel emissions and overall operating cost in aeronautical equipment. Despite wide applicability, the implementation of SMA technology into aerospace-related actuator applications is hindered by harsh environmental conditions, which necessitate extremely high or low transformation temperatures. The versatility of the NiTi-based SMA system shows potential for meeting these demanding material constraints, since transformation temperatures in NiTi can be significantly raised or lowered with ternary alloying elements and/or Ni:Ti ratio adjustments. In this thesis, the expansive transformation capabilities of the NiTi-based SMA system are demonstrated with a low and high-temperature NiTi-based SMA; each encompassing different stages of the SMA development process. First, exploratory work on the NiTiSn SMA system is presented. The viability of NiTiSn alloys as low-temperature SMAs (LTSMAs) was investigated over the course of five alloy heats. The site preference of Sn in near-equiatomic NiTi was examined along with the effects of solution annealing, Ni:Ti ratio adjustments, and precipitation strengthening on the thermomechanical properties of NiTiSn LTSMAs. Second, the thermomechanical processability of NiTiHf high-temperature SMA (HTSMA) wires is presented. The evolution of various microstructural features (grain size reduction, oxide growth, and nano-precipitation) were observed at incremental stages of the hot rolling process and linked to the

thermal and mechanical responses of respective HTSMA rods/wires. This work was carried out in an effort to optimize the rolling/drawing process for NiTiHf HTSMAs.

ACKNOWLEDGEMENTS

First and foremost, I would like to give thanks to my advising professor, mentor, and uncle Dr. Marcus L. Young for introducing me to Materials Science and Engineering. His continued guidance and support throughout my academic career at The University of North Texas (UNT) has greatly benefited my personal and intellectual development. I hope to pass on and apply the many things Marcus has taught me to my future colleagues and projects.

I would also like to thank my internship mentor, co-advisor, and research supporter Dr. Othmane Benafan for the numerous opportunities he's provided me. The internship projects and design challenge he so thoughtfully constructed have helped me realize my full potential and enabled my success. Othmane's passion for his field and devotion to advancing SMA technology has truly inspired me and shaped my career ambitions.

I'm thankful for the faculty of the Materials Science and Engineering Department at UNT for creating an encouraging environment to cultivate my education and prospective future. The untold knowledge I've absorbed from these professors over the past five years, defines my intellect, and (subjectively) qualifies this thesis.

I must also give thanks to my lab group members: Nathan Ley, and Matthew Carl for their generous help and advice, with which this thesis was made possible. Lastly, I appreciate my classmates: Keirsten Gomez, Tyler Torgerson, and Haley Barnes for their academic collaboration and friendship; as well as my parents and sister, McKenzie, for their unconditional encouragement.

TABLE OF CONTENTS

Page

CHAPTER 1.TABLE OF CONTENTS

LIST OF TABLES

Page

LIST OF FIGURES

Page

CHAPTER 1

INTRODUCTION AND BACKGROUND

1.1 Introduction

Shape memory alloys (SMAs) show promising potential in actuator applications for their unique ability to recover from large deformations into a predetermined shape with the simple addition of thermal or electrical heating [1-5]. SMAs offer an effective alternative to many industrial actuator applications due to their reduced system complexity relative to conventional actuator mechanisms [3]. Their lightweight, compact design provides potential for reducing fuel emissions and overall operating cost in aeronautical equipment. Additionally, since an SMA actuator is a single component device, the overall actuator is less prone to failure proving for a safer overall design.

Although these benefits remain apparent, the implementation of SMA technology into aerospace-related actuator applications has been sporadic [3-7]. Limitations arise from the harsh temperatures exposed to many aerospace devices, such as heat generated by turbine engines, or the frozen environments of the upper atmosphere and deep space. SMA actuators under these ambient conditions must exhibit extremely high or low transformation temperatures to ensure actuation occurs intentionally rather than through external temperature stimuli. To meet these demanding material constraints, significant progress has been made in expanding the operating temperatures of SMAs [3, 4].

Past efforts to raise/lower transformation temperatures in SMAs has proven the NiTi-based SMA system particularly versatile. The characteristic martensite-to-austenite phase transformation in NiTi-based SMAs is strongly influenced by ternary additions and/or Ni:Ti ratio

adjustments [8-11]. NiTi-based SMAs exhibit a wide range of transformation temperatures, from ~1000°C in the NiTiPt SMA system [10], to sub-cryogenic temperatures in NiTiFe SMAs [11]. These expansive transformation capabilities suggest the potential for NiTi-based SMAs in many aerospace actuator applications that necessitate extreme transformation temperatures.

The development and scale-up of NiTi-based SMA technology for high and low temperature actuator applications has seen varying degrees of progress; with some NiTi-based SMAs fully designed and entering system development [12], while other NiTi-based alloy systems are yet to be explored. In this thesis, both a low and high-temperature NiTi-based SMA system are presented and investigated; each encompassing different stages of the SMA development process.

First, exploratory work on the NiTiSn SMA system is presented. The viability of NiTiSn alloys as low-temperature SMAs (LTSMAs) was investigated over the course of five alloy heats (Heats I-V). The site preference of Sn in near-equiatomic NiTi was examined by substituting Sn for Ni in Heat I and Sn for Ti in Heat II up to 10 at.% Sn. The effects of solution annealing (Heat III), Ni:Ti ratio adjustments (Heat IV), and precipitation strengthening (Heat V) on the thermomechanical properties of NiTiSn SMAs were also evaluated.

Second, the thermomechanical processability of NiTiHf high-temperature SMA (HTSMA) rods is presented. NiTiHf HTSMA rods with an initial diameter of 6.35mm were hot-rolled at 700°C or 800°C to a final diameter of ~1mm over a series of 25 or 50 non-consecutive hot passes. The evolution of various microstructural features (grain size reduction, oxide growth, and nano-precipitation) were observed at incremental stages of the hot rolling process and linked to the thermal and mechanical responses of respective HTSMA rods/wires. These thermal, mechanical,

and microstructural properties were compared across both rolling temperatures (700°C & 800°C) in an effort to optimize the rolling/drawing process for NiTiHf HTSMA wires.

1.2 Phase Transformations in SMAs

The atomic structure of NiTi-based SMAs is generally composed of two dominant phases: martensite and austenite. The low temperature phase: martensite (B19'), typically exhibits a monoclinic crystal structure, but has also been observed in orthorhombic and tetragonal forms; while austenite (B2), the high temperature phase, is generally comprised of a more symmetrical cubic structure [2]. Phase transformation between these two crystal structures occurs via shear lattice distortion rather than atomic diffusion.

This diffusionless transformation can either be stress-induced, temperature-induced, or a combination of the two. SMAs exhibit three phenomena, which remain contingent on these influences: the shape memory effect, pseudoelastic effect, and two-way shape memory effect [2]. **Fig 1.1** illustrates these three effects and their relationship to phase transformations as a function of stress, strain, and temperature in NiTi-based SMAs.

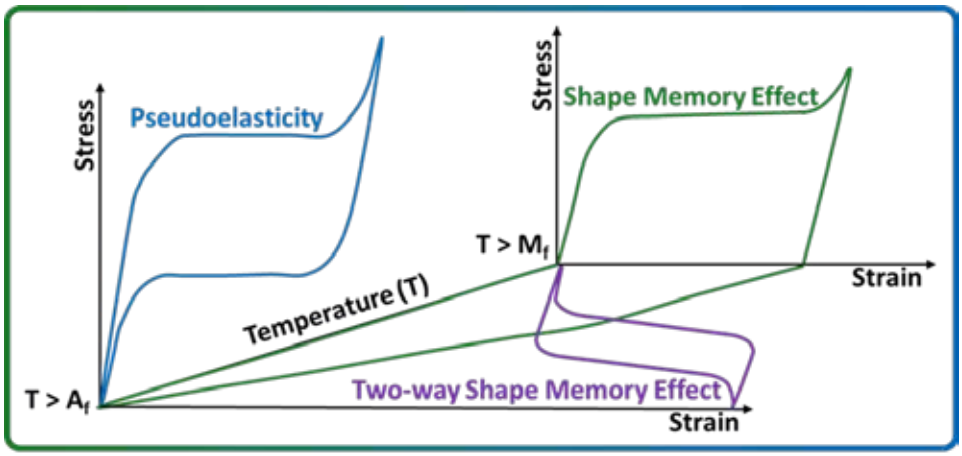

Fig. 1.1. The shape memory effect, pseudo-elastic effect, and two-way shape memory effect as a function of stress, strain, and temperature in NiTi-based SMAs.

When an SMA experiences a stress-induced phase transformation, this is known as the pseudoelastic effect. As stress is introduced to the material, the parent austenite phase transforms into the martensite phase to account for the stress and transforms back to austenite when the stress is removed. The pseudoelastic effect is often called the “super” elastic effect as it appears to demonstrate an extremely wide elastic modulus.

When an SMA experiences a temperature-induced phase transformation, this is known as the shape memory effect. When introducing stress to an SMA in the martensite phase, the material will “detwin” into different martensitic orientations. The SMA is considered permanently deformed until heat is introduced into the system; at which point, the detwinned martensite will transform into the austenite phase. When the SMA is cooled, the austenite will transform back into the original martensite orientation, thereby returning the material to its original shape prior to deformation.

Although the shape memory effect is described as a temperature-induced transformation, the process still requires stress to deform the SMA into detwinned martensitic variants. Since stress is necessary prior to heating to austenite, the process described in the paragraph above is more technically known as the one-way shape memory effect. However, some SMAs can exhibit a phenomenon known as the two-way shape memory effect, where both the austenite-to-martensite and martensite-to-austenite transformations are purely temperature-induced. The two-way shape memory effect is created by processing an SMA under controlled thermomechanical cycles. After these cycles, an SMA will remember its stress-induced shape at a specific temperature, even when no stress is present.

1.3 History of SMAs

In the late 19th century, non-reversible martensite was first observed in the FeC alloy system by A. Martens [13]. This metallurgical phenomenon sparked great interest in the scientific community and is attributed to the eventual discovery of reversible martensite in the CuZn and CuAl system [14]. The true potential of reversible martensite was not fully realized until 1963, when W. Buehler observed the phenomenon in the NiTi alloy system [15]. Unlike its predecessors, NiTi alloys exhibited mechanical properties on par with common engineering materials and demonstrated the potential of SMAs toward future engineering applications. In the following decades, the NiTi system was widely studied to further understand the effects of compositional variation (i.e. the Ni:Ti ratio) [8, 9, 16-19], processing [20-28], and ternary additions on the properties of NiTi-based SMAs.

1.4 Effects of Ni:Ti Ratio

It is well established that transformation temperatures in Ni-rich NiTi SMAs are extremely sensitive to stoichiometric variation. In the early years of NiTi SMA research, the effects of Ni:Ti ratio on transformation temperatures were heavily scrutinized but results yielded high experimental scatter [16-19]. Recent studies with improved experimental control and documentation have returned more definite conclusions [8, 9].

As Ni concentration increases past 49.8 at.% in NiTi SMAs, transformation temperatures decrease substantially as shown in region II of **Fig 1.2** [8]. This strong correlation can be attributed to an improved crystallographic compatibility between the martensite and austenite phases as Ni is added to the NiTi matrix.

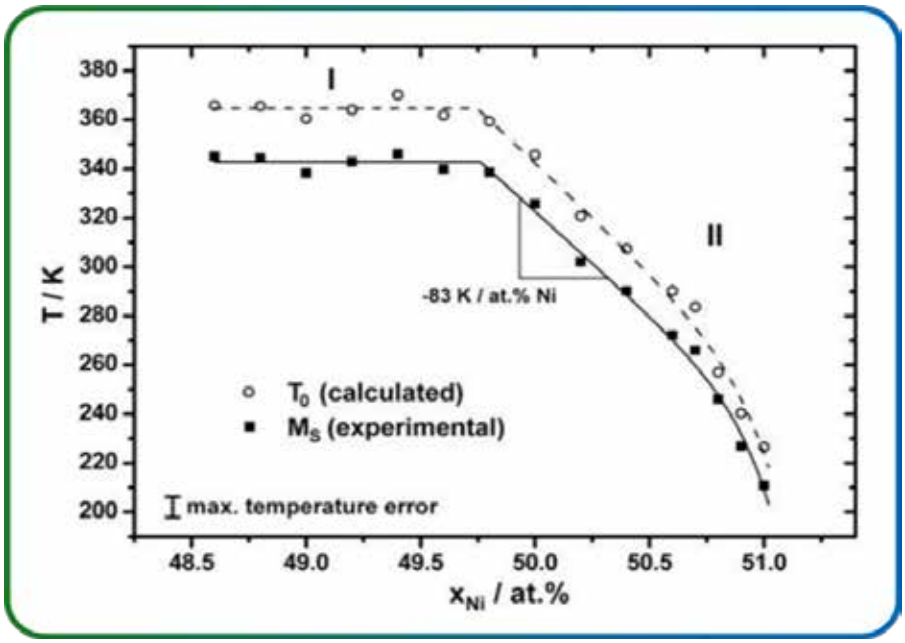

Fig. 1.2. The effects of nominal Ni content on recorded M_S in binary NiTi SMAs [8].

Since the atomic radius of Ni is less than that of Ti (1.49 Å < 1.76 Å), as additional Ni substitutes into the equiatomic NiTi matrix the lattice compresses. With a compressed lattice, less energy is needed to overcome the energy barrier between the parent and product phase during the martensitic transformation. Thus, phase transformations occur with less energy at lower temperatures.

An increase in Ni content has also been shown to decrease the thermal hysteresis width and heat of transformation [8]. These trends can be rationalized by the same mechanism described above. With improved lattice compatibility between the cubic and monoclinic structures, phase transformation occurs more easily, leading to less energy detected in calorimetry measurements.

With regards to Ti-rich NiTi, transformation temperatures remain unaffected by elevated Ti concentration. The NiTi phase diagram, shown in **Fig 1.3**, indicates that Ti is virtually insoluble in binary NiTi; so upon substitution, Ti_2Ni precipitates form which preserves the equiatomic

stoichiometry of the NiTi matrix, resulting in no transformation temperature shifts. This mechanism explains the transformation plateau in region I of **Fig 1.2** [8].

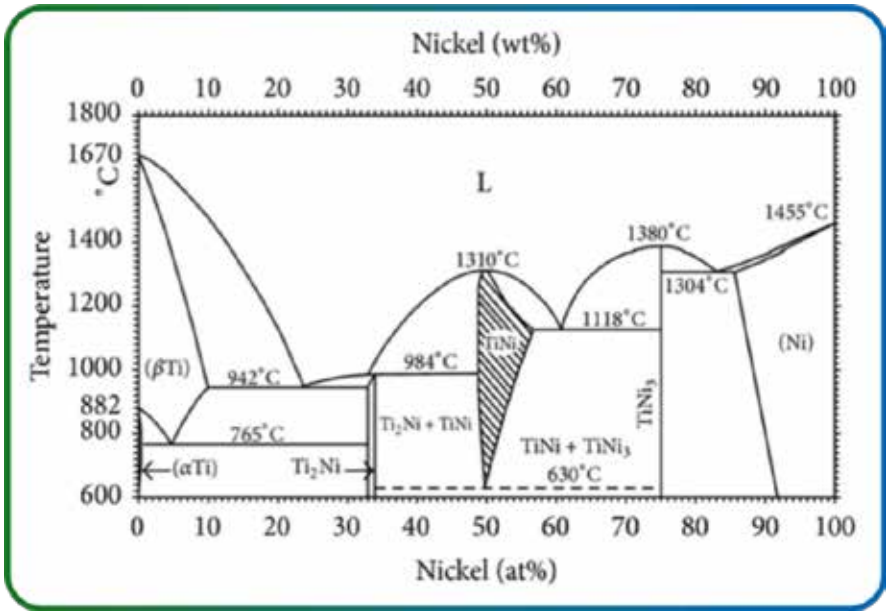

Fig. 1.3. Binary phase diagram for Ni and Ti [29].

1.5 Effects of Processing

The thermomechanical properties of NiTi-based SMAs can be altered in infinite ways by infinite means. From the myriad of processing techniques developed for SMAs in the past half-century, a small selection will be discussed to highlight several unique features of the binary NiTi SMA system.

Low temperature aging techniques are often utilized to fine-tune transformation temperatures and mechanical properties in NiTi-based SMAs. In Ni-rich NiTi, low temperature aging can promote Ni_4Ti_3 precipitation, which precisely removes Ni from the NiTi matrix, raising transformation temperatures while simultaneously inducing precipitation strengthening to improve SMA performance [21, 28].

The thermomechanical properties of NiTi-based SMAs are notably affected by oxygen and carbon, which should be considered when ensuring alloy purity during processing [20, 24]. Ti is inclined to react with these elements (O and C), forming $Ti_4Ni_2O_x$ and TiC precipitates, respectively. Both of these precipitates pull Ti out of the NiTi matrix, increasing the SMA's Ni:Ti ratio, which consequently lowers transformation temperatures. $Ti_4Ni_2O_x$ and TiC are difficult to remove from the material since each phase has a higher melting temperature than the parent NiTi matrix.

When cold rolling NiTi SMAs in the martensitic state, new martensitic variants form through the typical "detwinning" process, along with stress-induced dislocations/vacancies [22, 25]. Both the deformed martensite and point defects work to stabilize the martensite, hindering reverse transformation (B19' à B2) upon the first heating cycle, thus increasing A_S and A_F. The effects of martensite stabilization diminish with the first cooling cycle as austenite transforms to familiar martensite orientations via the two-way shape memory effect. However, the point defects generated during the initial cold roll remain intact and permanently elevate A_S and A_F [22, 25].

To elaborate on martensite stabilization from a thermodynamic perspective, the elastic strain energy stored in martensite should be considered. The thermodynamic equilibrium for a martensite plate and the austenite phase is formulated in **Eq. 1.1**, where g_A and g_M represent the chemical free energy of the austenite and martensite, respectively, and Δg_{el} represents the elastic strain energy stored around the martensite plate [23].

$$2\Delta g_{el} + (g_A - g_M) = 0 \quad \text{(Eq. 1.1)}$$

The elastic strain energy stored in martensite promotes reverse transformation (B19' à B2) and resists forward transformation (B2 à B19') [23, 25]. When the martensite deforms during the initial cold roll, the elastic strain relaxes. Therefore, with less elastic strain to assist reverse transformation, the material requires more energy to transform to austenite, and thus, A_S and A_F occur at higher temperatures.

In addition to the previously described effects, cold rolling can also reduce grain size [26]. As grain size decreases in binary NiTi, the martensitic reorientation of forward transformation becomes increasingly confined by grain boundaries [26]. With less space for the self-accommodated martensitic variants to form, forward transformation is suppressed, and M_S and M_F shift to lower temperatures.

While cold rolling reduces grain size in NiTi SMAs, annealing promotes grain growth [26, 27]. The effects of annealing on phase transformation behaviors in NiTi SMAs directly contrast the effects of cold rolling [27]. Therefore, the employment of these two processing techniques can effectively control the grain size and consequent transformation temperatures in NiTi SMAs.

1.6 Effects of Ternary Additions

The first investigation on the effects ternary additions to NiTi SMAs was conducted in 1965 by F. Wang [30] who noted a significant decrease in transformation temperatures when alloying Co or Fe to equiatomic NiTi. Ten years later, Au, Al, Zr, and Mn were added to NiTi by K.H. Eckelmeyer [31] whose findings indicate alloy transformation temperatures can also be elevated with certain ternary elements. In 1978, the first major study on the NiTiCu alloy system

was performed by K.N. Melton and O. Mercier [32]. Their results suggested Cu addition narrows the stress hysteresis of transformation but has no effect on transformation temperatures.

Past research has built upon those pioneering studies as scientists work to fully explore the potential of NiTi-based SMAs. Researchers have alloyed NiTi with 36 different elements and produced over 1000 publications on ternary NiTi-based SMAs (**Fig 1.4**). From the comprehensive results of these publications, each of the 36 ternary elements can be categorized by their generalized effects on transformation temperatures in NiTi: 1) elements known to raise transformation temperatures, 2) elements known to lower transformation temperatures, or 3) elements with neutral or unconfirmed effects on transformation temperatures.

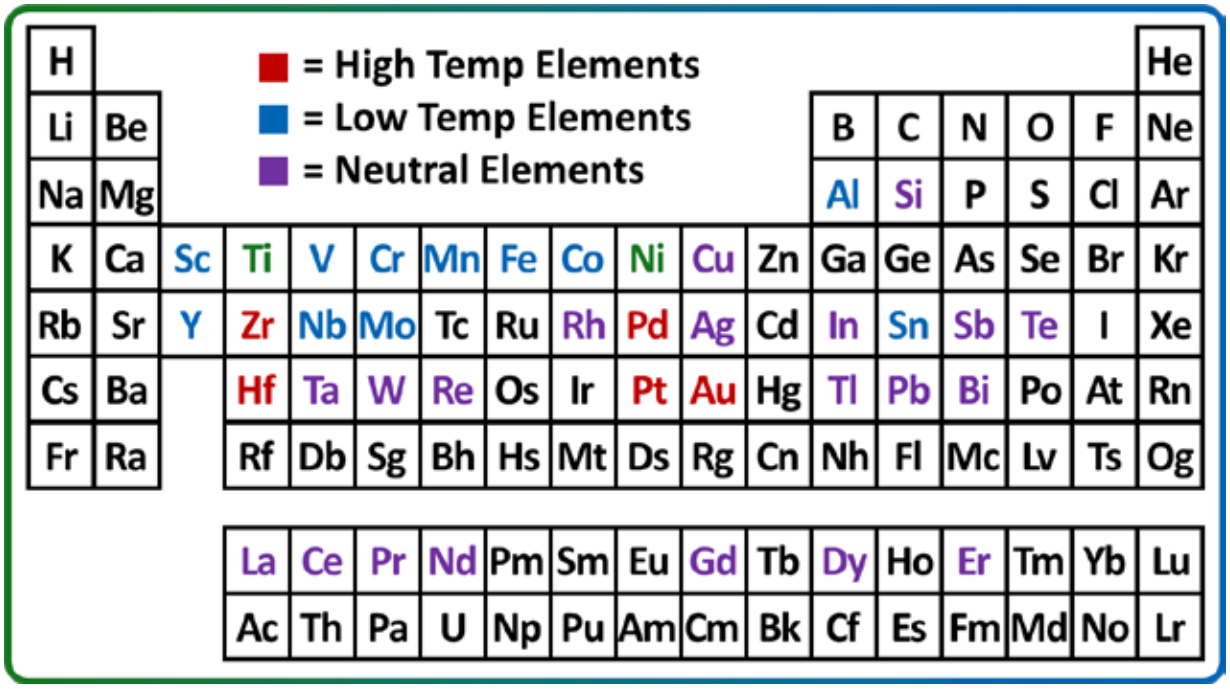

Fig. 1.4. The periodic table displaying all 36 NiTi-based ternary SMA systems studied to-date. Each NiTi-based SMA system is represented by a respective ternary element which is colored based on the element's generalized effects on transformation temperatures in NiTi. Elements known to raise transformation temperatures when alloyed to NiTi are labeled in red, those known to lower transformation temperatures are shown in blue, and those with neutral or unconfirmed effects are presented in purple.

The fundamental reasons behind transformation temperature shifts when adding ternary elements to NiTi SMAs is not firmly established. Theory suggests that transformation is dependent on the elastic constants of the two phases in the material which must overcome a critical value to induce transformation [2, 33]. Since alloy composition and temperature affect the elastic modulus of an SMA, then both factors clearly influence transformation. However, the effects of various alloying elements on the elastic properties of NiTi-based SMAs is rather complicated given the nature of pseudoelasticity. Thus, to elucidate the complexities of the elastic modulus in NiTi-based SMAs, the effects of alloying elements on atomic bonding should be considered. In metallically bonded materials, atoms are held together by delocalized electrons, or valence electrons. Therefore, understanding how the electronic structure of NiTi-based SMAs is altered by alloying elements could help clarify the mechanisms affecting transformation temperatures.

In a 2008 study by M. Zarinejad [33], the electronic structures of various NiTi-based SMAs were examined by comparing transformation temperatures to valence electron concentrations in respective alloys. Valence electron concentration (c_v) was calculated as the valence electrons in the material (e_v) divided by the total electrons in the material (e_t). The expanded formula is presented in **Eq. 1.2**, where $f_{Ni}/f_{Ti}/f_X$ represent the atomic fraction of Ni, Ti, and a ternary element in the SMA, respectively; and $Z_{Ni}/Z_{Ti}/Z_X$ denote the atomic numbers of each respective element.

$$c_v = \frac{e_v}{e_t} = \frac{f_{Ni}e_v^{Ni} + f_{Ti}e_v^{Ti} + f_X e_v^X}{f_{Ni}Z_{Ni} + f_{Ti}Z_{Ti} + f_X Z_X} \quad \text{(Eq. 1.2)}$$

Fig 1.5, displaying c_v vs. M_S, indicates an inverse correlation between transformation temperatures and valence electron concentration [33]. In other words, NiTi-based SMAs with lower transformation temperatures contain more valence electrons and vice versa. Valence

electrons help to bind atoms together, so as c_v increases, atoms are bound more tightly, and the elastic modulus of the material increases [34]. It is known that the stored elastic energy of a NiTi-based SMA promotes reverse transformation (B19' à B2) and inhibits forward transformation (B2 à B19') [23, 25]. Therefore, as the stored elastic energy in a NiTi-based SMA increases due to a higher c_v, reverse transformation occurs more readily at lower temperatures.

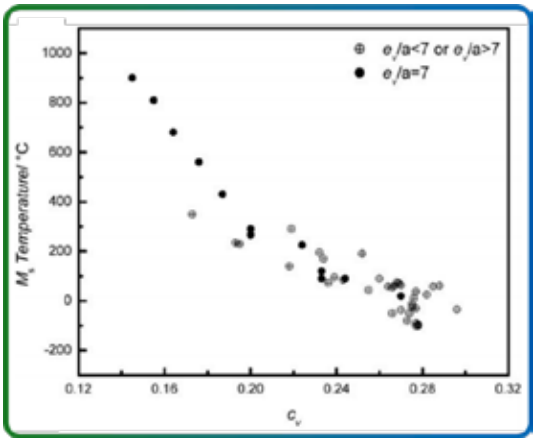

Fig. 1.5. The influence of the valence electron concentration (c_v) on M_s in various ternary and quaternary NiTi-based SMAs surveyed from literature [33].

While valence electron concentration clearly correlates with transformation temperatures in NiTi-based SMAs, it is certainly not the sole contributor to these observed trends. The atomic size of alloying elements would understandably affect transformation temperatures in NiTi-based SMAs as well. In NiTiHf and NiTiZr SMAs, for example, Hf and Zr exhibit a site preference for Ti lattice sites because all three elements have an HCP crystal structure and similar electronic structure. Although, since Hf and Zr have larger atomic radii than Ti (Ti - 1.76 Å < Zr - 2.06 Å < Hf - 2.08 Å), when Hf or Zr are substituted into NiTi, the material's lattice and consequent unit volume expand. If the atomic rearrangement and volume change associated with martensitic transformation is considered, an SMA with a larger unit volume will require more energy to compensate this volume change, thus shifting transformation to higher

temperatures. This principle can be translated to LTSMA systems such as NiTiSn as well. Sn substituted into NiTi will substitute into Ti lattice sites, compressing the lattice due to a smaller atomic radius (1.45 Å < 1.76 Å). Thus, lowering transformation temperatures as less energy is needed to account for the volume change of transformation.

Atomistic modeling and experimental findings indicate that ternary additions to NiTi exhibit a site preference for either Ni or Ti lattice sites. **Fig 1.6** displays the site preference of 34 ternary elements in Ni-rich and Ti-rich NiTi SMAs, respectively [35]. These elemental dispositions were calculated through density functional theory (DFT) modeling, by substituting single atoms of ternary elements into a 32-atom austenitic NiTi lattice ($Ni_{15}Ti_{16}X$ & $Ni_{16}Ti_{15}X$, where X represents a single atom of ternary element). The generalized trends from this calculation suggest: elements near the center of the transition metals substitute for Ni lattice sites, while elements near the edge substitute for Ti lattice sites. Most alloys from literature were synthesized with these substitution rules in mind, since non-preferential ternary substitutions to NiTi typically form intermetallic compounds that impair SMA performance.

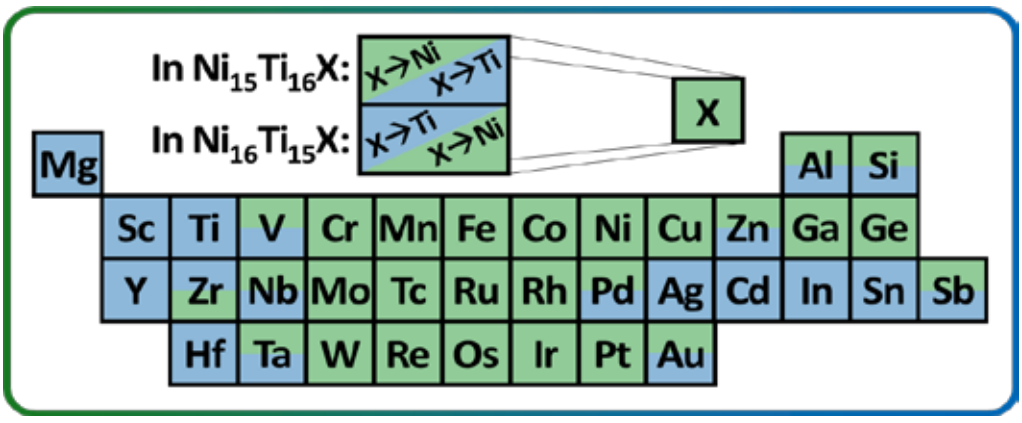

Fig. 1.6. DFT calculations indicating the site preference of 34 ternary elements in NiTi SMAs [35]. Note: The bottom half of each element box is designated to Ni-rich NiTi ($Ni_{16}Ti_{15}X$) while the top half belongs to Ti-rich NiTi ($Ni_{15}Ti_{16}X$), where X is the single element being added to the system. If the box section is blue, the ternary element substitutes for Ti; if the box section is green, the ternary element substitutes for Ni.

1.7 NiTiSn SMAs

The NiTiSn SMA system has received some research attention [36-46] but remains relatively unexplored and undeveloped. While NiTiSn SMAs are still in the very early stages of the SMA development process, some progress has been made. The NiTiSn SMA system was first investigated in 2004 by Zheng et al. [36] who reported a martensitic transformation upon cooling with no intermediate R-phase in $Ni_{47.5}Ti_{47.5}Sn_5$ and $Ni_{45}Ti_{45}Sn_{10}$ alloys. A three-step transformation (B2 à R à B19') upon cooling and two-step transformation (B19' à B2) upon heating was later detected in $Ni_{50-2x}Ti_{50+x}Sn_x$ melt-spun ribbons [37, 38]. The microstructures of these ribbons contained a Ti_3Sn lamellar phase that became more prevalent at higher Sn concentrations. Annealing a $Ni_{36}Ti_{57}Sn_7$ melt-spun ribbon was shown to decrease transformation temperatures and thermal hysteresis [39, 40]. In $Ni_{50-2x}Ti_{50+x}Sn_x$ alloys, the two-way shape memory effect was found to improve with Sn addition while fracture strength and elongation decreased [41]. The effects of site preference on alloy properties was examined in a $Ni_{50}Ti_{49}Sn_1$ and $Ni_{49}Ti_{50}Sn_1$ alloy [42]. This study observed a more pronounced decrease in transformation temperatures when substituting Sn into Ti lattice sites relative to Sn in Ni sites.

A ternary diagram of the NiTiSn SMA system, presented in **Fig 1.7**, denotes, to the authors' knowledge, every nominal composition investigated throughout NiTiSn literature to date [36-46]. This diagram suggests that the NiTiSn SMA system has only been partially explored since past research has substituted Sn into Ni lattice sites almost exclusively. Since DFT modeling suggests Sn's absolute preference for Ti lattice sites, and $Ni_{50}Ti_{49}Sn_1$ [42] exhibits promising thermal properties, it becomes apparent that the $Ni_{50}Ti_{50-x}Sn_x$ SMA system requires a full-scale investigation.

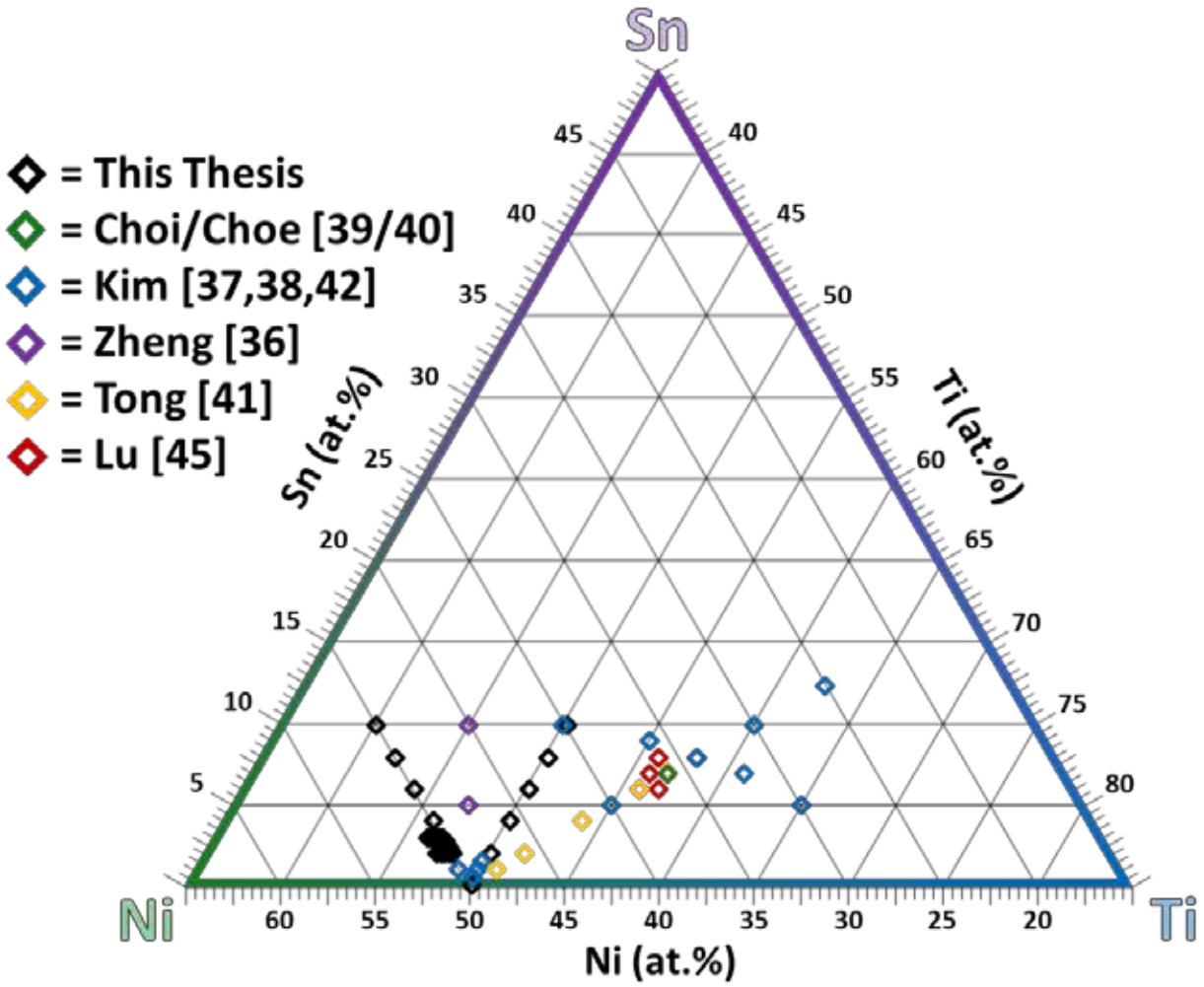

Fig. 1.7. An abbreviated Ni-Sn-Ti ternary plot displaying all nominal compositions investigated throughout literature to date for the Ni-Sn-Ti SMA system (to the authors' knowledge).

1.8 NiTiHf SMAs

The potential for NiTiHf SMAs in high temperature actuator applications was first realized in 1992 [47]. The NiTiHf SMA system has generated considerable commercial interest in the last decade due to the low cost of Hf relative to other high temperature alloying additions such as Au, Pd, and Pt. For this reason, NiTiHf SMAs have been researched extensively [9, 35, 47-280] in efforts to develop and scale-up NiTiHf HTSMA actuator technology for real-world applications.

With the bulk thermomechanical properties of the NiTiHf HTSMA system firmly established, research and development has shifted towards processing bulk NiTiHf material into functional HTSMA actuators. While NiTi-based SMAs can be processed into numerous forms (wires, ribbons, rings, tubes, plates, etc.) using conventional metal forming processes (extrusions, forging, rolling) [3], only details on the fabrication of NiTiHf HTSMA wires will be discussed for the purposed of this thesis.

The thermomechanical processability of NiTiHf wires poses several challenges involving the reactivity of Hf/Ti, grain refinement, and nano-precipitation [261, 281-283]. NiTiHf SMAs are sensitive to oxygen and carbon impurities due to the reactivity of Ti and Hf. Therefore, to ensure alloy purity during processing, open-air heat treatments should be minimized to limit material oxidation. While Ti-rich NiTiHf exhibit stable transformation temperatures, their reactivity and poor transformation behavior motivated a shift in research focus to Ni-rich NiTiHf [124]. The processability of Ni-rich compositions brought about additional complications as Ni-rich NiTiHf are susceptible to H-phase nano-precipitation [281, 283]. H-phase precipitates strengthen the material at the expense of ductility, reducing the formability of the material and impairing thermomechanical processability.

Despite these difficulties, the thermomechanical processability of NiTiHf HTSMAs was first demonstrated in a $Ni_{50}Ti_{35}Hf_{15}$ wire hot extruded in a stainless steel jacket at 900°C and wire drawn [261]. The 0.75 mm diameter wire exhibited cyclic stability and adequate mechanical properties, with a transformation temperature decrease of ~15°C due to processing. While this wire was processed successfully, the wire drawing process for NiTiHf HTSMAs is far from optimized and requires further inquiry; hence, it is the subject of one chapter of this thesis.

CHAPTER 2

EXPERIMENTAL PROCEDURES

2.1 Procedures Overview

The contents of this thesis can be separated into two main themes: 1) the development of NiTiSn LTSMAs, and 2) the processing optimization of NiTiHf HTSMAs. Since each theme is inherently unique and encompasses different stages of the SMA design process, the methodology for each theme will be presented independently.

2.2 NiTiSn Low-Temperature SMAs

The NiTiSn ingots produced in this thesis were prepared from: high purity electrolytic nickel anodes (99.99 wt.% Ni) and tin ingots (99.9 wt.% Sn) purchased from King Supply Inc. (Franklin Park, IL, USA) and titanium pellets (99.9 wt.% Ti) purchased from Zirconium Research Corp. (Philomath, OR, USA). The Ni and Ti were cold-rolled, sectioned, and electro-sonically cleaned to remove surface contaminants. The Sn ingots were partitioned by melting each ingot in air to form 1-3 g Sn droplets. To ensure accurate melt compositions, raw material segments were ground within ± 0.001 g of the intended stoichiometry. Additionally, alloys from Heats IV-V were produced from ≈ 40 g of raw material to ensure precise Ni content variation between each ingot. Raw materials were carefully weighed using a Scientech ZSA 120 analytical balance to a ± 0.001 g precision.

NiTiSn alloys were prepared with an Edmund Bühler GmbH vacuum arc melter on a water-cooled copper hearth. In the cigar-shaped copper mold, Ni sheets were placed above the more reactive Ti and Sn to help prevent material loss during the melt process. To remove oxygen from

the melt environment, the chamber was first evacuated to a pressure of 2 ª 10^{-2} mbar and back-flushed with argon to 800 mbar. This step was repeated five times at which point the chamber was vacuum pumped down to 8 ª 10^{-5} mbar and Ar back-filled to 600 mbar. Lastly, a high purity Ti getter (99.9 wt.%) was held in a molten state for 30 seconds to remove residual oxygen content from the melt chamber. The plasma arc current was set between 180 and 200 A for the initial melt to help prevent material loss. After the first arc-melt, the alloys were flipped and re-melted five times with an arc current between 200 and 250 A to ensure homogeneous elemental distribution.

Final castings were heat treated in a Ney Vulcan D-1750 open air box furnace to solutionize and precipitate alloys under parameters specific to each heat. These processing parameters, as well as the nominal compositions of the 24 NiTiSn ingots produced in this thesis, are shown in **Table 2.1**. After heat treatments, the oxide layers formed on each alloy (**Fig 2.1**) were removed by polishing. A wire-cut electrical discharge machine (EDM) was utilized for all necessary sample sectioning. To prepare for microstructural characterization, samples were mechanically polished with SiC paper and diamond-suspension polishing pads to a resolution of 0.01 µm. SEM images were captured with a Hitachi TM3030Plus tabletop microscope equipped with EDS to evaluate alloy chemical composition. EDS point spectra were recorded for 2 ª 10^5 counts at five locations on each alloy. Beam intensity and working distance were set to 20 keV and 8.5 ± 1.0 mm, respectively to provide a statistically accurate analysis [284].

Table 2.1. The nominal compositions, heat treatment parameters, and pre/post-melt masses of the 24 NiTiSn SMAs produced in Heats I-V. With regards to alloy cooling processes, "FC" indicates the alloy was furnace cooled while "WQ" signifies water quenching.

Heat #	Elemental Compositions	Pre-Melt Mass (g)	Post-Melt Mass (g)	Heat Treatment Parameters: Temperature	Time	Cooling
I	$Ni_{49.8}Ti_{50.2}$	27.71		1000°C	0.5hr	WQ
	$Ni_{47.8}Ti_{50.2}Sn_2$	27.5				
	$Ni_{45.8}Ti_{50.2}Sn_4$	29.74				
	$Ni_{43.8}Ti_{50.2}Sn_6$	28.90				
	$Ni_{41.8}Ti_{50.2}Sn_8$	29.31				
	$Ni_{39.8}Ti_{50.2}Sn_{10}$	28.49				
II	$Ni_{49.8}Ti_{48.2}Sn_2$	23.3		1000°C	0.5hr	WQ
	$Ni_{49.8}Ti_{46.2}Sn_4$	26.52				
	$Ni_{49.8}Ti_{44.2}Sn_6$	23.95				
	$Ni_{49.8}Ti_{42.2}Sn_8$	23.85				
	$Ni_{49.8}Ti_{40.2}Sn_{10}$	24.48				
III	$Ni_{49.8}Ti_{50.2}$	27.71		1000°C	24hr	WQ
	$Ni_{49.8}Ti_{48.2}Sn_2$	23.3				
	$Ni_{49.8}Ti_{47.95}Sn_{2.25}$	23.42	23.40			
	$Ni_{49.8}Ti_{47.7}Sn_{2.5}$	25.01	24.99			
	$Ni_{49.8}Ti_{47.45}Sn_{2.75}$	25.25	25.24			
	$Ni_{49.8}Ti_{47.2}Sn_3$	25.27	24.98			
	$Ni_{49.8}Ti_{46.2}Sn_4$	26.52				
	$Ni_{49.8}Ti_{44.2}Sn_6$	23.95				
	$Ni_{49.8}Ti_{42.2}Sn_8$	23.85				
	$Ni_{49.8}Ti_{40.2}Sn_{10}$	24.48				
IV	$Ni_{50.8}Ti_{48.2}Sn_1$	38.59	38.57	1000°C	24hr	WQ
	$Ni_{50}Ti_{48}Sn_2$	41.09	41.06			
	$Ni_{50.2}Ti_{47.8}Sn_2$	39.83	39.81			
	$Ni_{50.4}Ti_{47.6}Sn_2$	39.66	36.63			
	$Ni_{50.6}Ti_{47.4}Sn_2$	41.32	41.26			
	$Ni_{50}Ti_{47}Sn_3$	35.82	35.80			
	$Ni_{50.2}Ti_{46.8}Sn_3$	34.93	34.91			
	$Ni_{50.4}Ti_{46.6}Sn_3$	37.45	37.41			
	$Ni_{50.6}Ti_{46.4}Sn_3$	36.22	35.91			
V	§ $Ni_{50.6}Ti_{47.4}Sn_2$	41.32	41.26	1000°C, 24hr, WQ	500°C	12hr / 24hr / 60hr, WQ
	§ $Ni_{50.4}Ti_{46.6}Sn_3$	37.45	37.41		550°C	12hr / 24hr / 60hr, WQ
	§ $Ni_{50.6}Ti_{46.4}Sn_3$	36.22	35.91		650°C	12hr / 24hr / 60hr, WQ
	§ - These 3 alloys were aged at all 3 times & temps (9 respective heat treatments).					
V	$Ni_{50.8}Ti_{48.2}Sn_1$	38.59	38.57	1000°C, 24hr, WQ	550°C	1hr, FC
					650°C	1hr, FC
					750°C	1hr, FC
					850°C	1hr, FC

Samples were prepared for thermal analysis by EDM sectioning 5 mm Ø discs approximately 1 mm thick and polishing off EDM residue. These alloy discs were characterized with a TA Instruments Q1000 DSC located at NASA Glenn Research Center (Cleveland, Ohio). Each sample underwent three thermal cycles from 150°C to -175°C at a standard heating/cooling rate of 10°C min^{-1} [285]. The austenite and martensite start and finish temperatures (A_S, A_F, M_S, and M_F, respectively) were calculated using the tangent-intercept method. Thermal hysteresis (Δ_{TH}) and full width (ΔT_{FW}) were defined as (A_F-M_S) and (A_F-M_F) respectively.

A Tukon 2500 Vickers hardness tester was utilized to evaluate alloy hardness. Five indentations were made with a 300 g applied load for 10 seconds near the center of each alloy cross-section (**Fig 2.1**). Vickers hardness values (HV) were extracted from the micro-indentations using standard calculations [286].

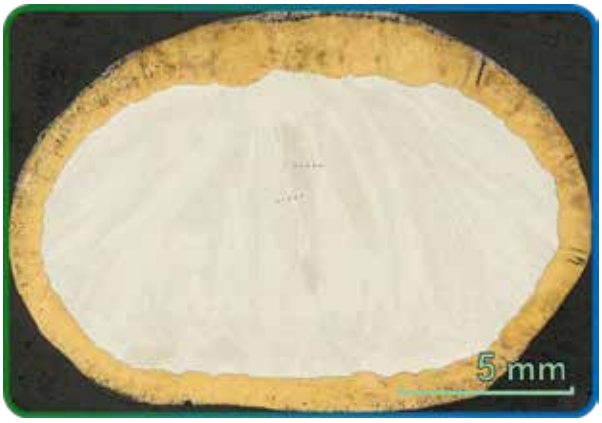

Fig. 2.1. Optical image of the cross-section of a $Ni_{49.8}Ti_{47.7}Sn_{2.5}$ SMA (annealed at 1000°C for 24 hours) indicating the general location of Vickers hardness indentations and oxide layers.

2.3 NiTiHf High-Temperature SMAs

The NiTiHf HTSMAs utilized in this thesis were commercially produced over two alloy heats via vacuum induction skull melting by Flowserve (Ohio, USA) and provided to UNT via NASA Glenn Research Center (Cleveland, OH, USA) for study. The ingots were vacuum homogenized at

1050°C for 72 hours followed by hot-extrusion at 900°C. The hot-extruded rods were machined down to a diameter of 6.35 mm sectioned every 50.8 mm. These dimensions (6.35 mm Ø × 50.8 mm l) represent the as-received geometry of the HTSMA rods used in this thesis.

As stated previously, the NiTiHf rods originate from two separate melts, formally denoted as Flowserve's (FS5, & FS6). **Table 2.2** indicates the elemental compositions of these melts and the processing conditions of the five HTSMA rods hot-rolled in this thesis.

Table 2.2. The alloy melts, elemental compositions, and processing conditions of the five HTSMA rods hot-rolled in this thesis. Processing conditions include: the hot-rolling temperature, the final diameter of the rod/wire, and the number of hot passes the material underwent to achieve that final diameter.

Alloy Melts	Composition (at.%)	Hot Roll Temp. (°C)	Total Passes	Final Ø (mm)
NiTiHf20 FS#5	$Ni_{50.8}Ti_{29.2}Hf_{20}$	700°C	25	1.00
		800°C	25	1.00
NiTiHf20 FS#6	$Ni_{50.7}Ti_{29.4}Hf_{19.9}$	700°C	25	1.11
			50	1.08
		800°C	25	1.06

At the start of the hot-rolling process, each rod was held in an Orton SentryXpress4.0 open-air box furnace at 700°C or 800°C for 30 minutes. The preheated rod was then passed through a room-temperature Durston 1.5 HP rolling mill and reduced to an approximate final diameter of 1 mm over the course of 25 or 50 non-consecutive passes. After each pass the rod was reheated to 700°C or 800°C for 5 minutes to alleviate residual strain and prepare the rod for the next pass. A section of the rod was removed every five passes for characterization, totaling five samples per rod (5^{th}, 10^{th}, 15^{th}, 20^{th}, & 25^{th} passes or 10^{th}, 20^{th}, 30^{th}, 40^{th}, & 50^{th} passes). After each of these sectioning intervals, the rod was placed into the furnace for 30 minutes (rather than 5 minutes), before the hot-rolling process resumed. Note: the samples removed from the rods did not receive any additional thermal holds and are considered in the as-rolled condition.

A Hitachi TM3030Plus tabletop SEM equipped with EDS was utilized to observe how various microstructural features (grain size, oxide growth, and precipitate formation) evolved across the five documented stages of the hot-rolling process. Samples were mechanically polished in the cross-sectional direction with SiC paper to a 15 µm resolution and vibro-polished for ~12 hours in a Buehler VibroMet 2 with 0.25 µm colloidal silica suspension. The thickness and composition of the native oxide layer enveloping each sample was assessed with SEM imaging and EDS line spectra, respectively. Beam intensity and working distance were set to 20 keV and 8.5 ± 1.0 mm, respectively to ensure a statistically accurate analysis [284]. To effectively observe the size and orientation of the martensitic grains present in each SMA, samples were exposed to Kroll's etchant (25 mL $C_3H_8O_3$/6 mL HNO_3/1 mL HF^-) for 20 seconds. The grain size of each sample was calculated as the average length of 50 grains measured lengthwise.

The transformation temperatures of the NiTiHf HTSMA rods were determined using a Netzch DSC 204 F1 Phoenix machine. DSC samples were sectioned via EDM from the cross-sectional center of the parent rod, polished to a mass between 20 and 60 mg, electro-sonically cleaned, and subjected to three thermal cycles between 0°C and 400°C at a standard heating/cooling rate of 10°C min^{-1} [285]. A_S, A_F, M_S, and M_F were calculated from the third thermal cycle of each test using the tangent-intercept method.

CHAPTER 3

RESULTS AND DISCUSSION

3.1 NiTiSn Low-Temperature SMAs

To assess the viability of NiTiSn alloys in low-temperature actuator applications, the thermal and mechanical properties of the NiTiSn SMA system were explored over a series of five alloy heats (Heats I-V). The main goal was to produce a NiTiSn SMA that exhibits tunable, low temperature phase transformation behaviors. To demonstrate precise tunability, a target austenite finish temperature of -150°C was pursued for the final alloy design. Site preference was examined by substituting Sn for Ni (Heat I) and Sn for Ti (Heat II) in the NiTi-based SMA system. The effects of solution annealing (Heat III), Ni:Ti ratio adjustments (Heat IV), and precipitation strengthening (Heat V) on the thermomechanical properties of NiTiSn SMAs are also presented.

3.1.1 Heats I-II – Site Preference of Sn in NiTi

Nearly all NiTiSn SMAs studied throughout literature [36-42] were produced assuming Sn substitutes into Ni lattice sites rather than Ti lattice sites. This alleged site preference is supported by two of the Hume Rothery rules. Since Sn has an atomic radius of 1.45 Å, it is expected to more readily substitute for 1.49 Å Ni atoms over 1.76 Å Ti atoms. Furthermore, Ni and Sn exhibit nearly identical electronegativities (1.91 and 1.96, respectively) relative to Ti (1.54). However, the electronic structures of these elements suggest Sn should prefer Ti lattice sites over Ni. Both Sn and Ti prefer to give away two electrons to reach a lower energy full shell state, specifically $4d^{10}$ and $4s^2$ respectively, while Ni prefers to gain two electrons. Lastly, the intrinsic crystal structures of all three elements differ which offers little insight. Due to these discrepancies and limited

research [42] in the $Ni_{50}Ti_{50-x}Sn_x$ SMA system, the absolute site preference of Sn in near-equiatomic NiTi required further inquiry.

In the first two alloy heats, Sn was substituted for Ni in Heat I and Ti in Heat II. Since transformation temperatures are extremely sensitive to NiTi ratio adjustments in Ni-rich NiTi [8], the Ni:Ti ratio of Heats I-III was kept slightly Ti-rich (50.2 at.%) to remain on the transformation temperature plateau and isolate the influence of Sn on transformation behavior. The initial heat treatment for these alloys was relatively limited (1000°C for 30 minutes) to prevent excessive oxidation. The compositions and processing conditions of all alloy heats is provided in **Table 2.1**.

Fig 3.1a displays the microstructures of Heats I and II with Sn content up to 10 at.%. **Fig 3.1b** displays EDS maps for a region of a $Ni_{43.8}Ti_{50.2}Sn_6$ SMA, indicating the elemental distribution throughout respective phases in the microstructure. When substituting Sn for Ni (Heat I), a darker phase (i), identified as the parent NiTi matrix, contains significantly less Sn than intended due to its desegregation into a TiSn-rich lamellar phase (ii), which forms even in the 2 at.% Sn alloy and becomes progressively more prevalent at higher Sn concentrations. A less apparent third phase (iii), noted throughout the lamellar phase, can be distinguished by its slightly darker color and blurred phase boundaries. These blurred boundaries are most likely due to smearing caused by polishing and suggest the phase is slightly softer than the lamellar structure. Based on the EDS measurements presented in **Fig 3.2**, the lamellar phase exhibits a $NiTi_3Sn$ stoichiometry, while the third phase more closely resembles a $Ti_3(Sn,Ni)$ stoichiometry similar to those found in literature [36-42]. Much like the lamellar $NiTi_3Sn$ phase, the volume fraction of the $Ti_3(Sn,Ni)$ phase increases as a function of Sn content, although it disappears past 6 at.% Sn. Although the

EDS measurements and previous research on similar alloys suggests these phases ($NiTi_3Sn$, $Ti_3(Sn,Ni)$), other techniques such as X-ray diffraction are needed to confirm the exact stoichiometric ratios and crystallographic structures.

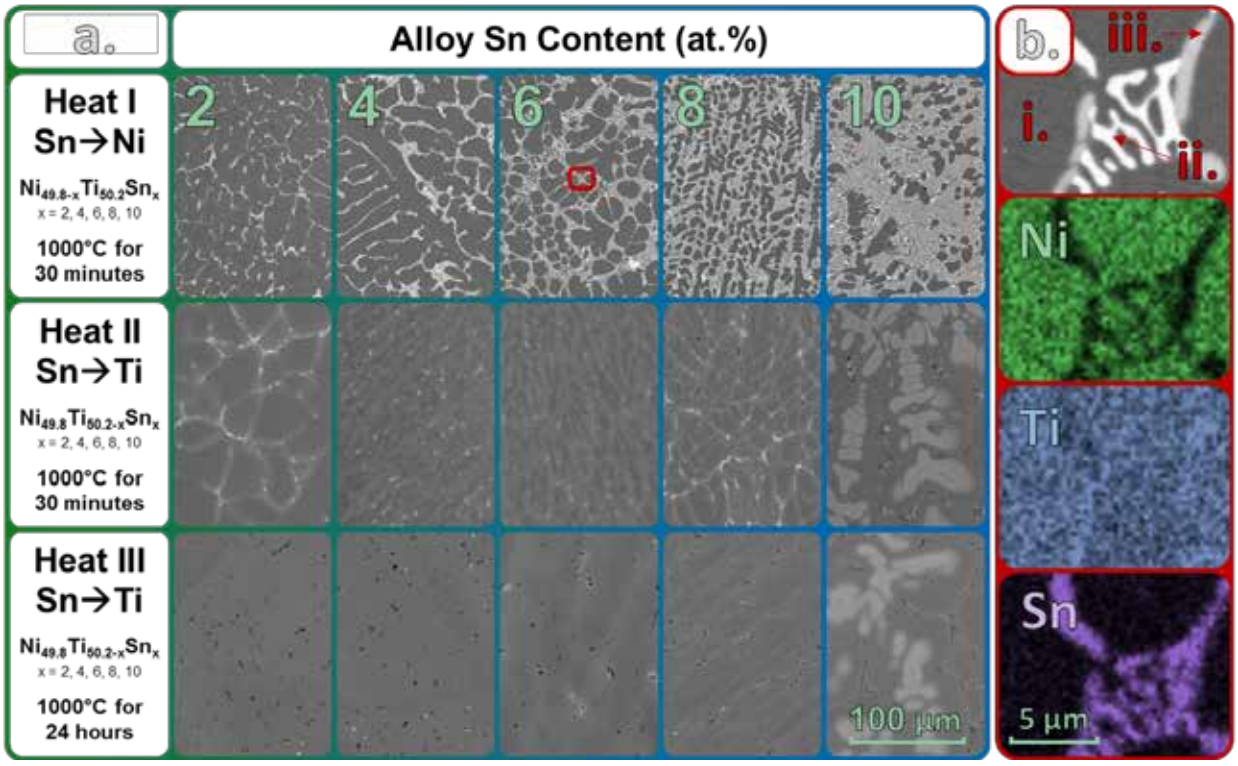

Fig. 3.1. (a) Microstructures of NiTiSn SMAs at 2, 4, 6, 8, and 10 at.% Sn, substituting Sn for Ni in Heat I ($Ni_{49.8-x}Ti_{50.2}Sn_x$/1000°C for 30 minutes), Sn for Ti in Heat II ($Ni_{49.8}Ti_{50.2-x}Sn_x$/1000°C for 30 minutes), and Sn for Ti in Heat III ($Ni_{49.8}Ti_{50.2-x}Sn_x$/1000°C for 24 hours). **(b)** EDS mapping for a region of a $Ni_{43.8}Ti_{50.2}Sn_6$ SMA, indicating the elemental distribution throughout respective phases in the microstructure.

The SEM images from Heat II SMAs, i.e. substituting Sn for Ti, exhibit much more homogeneous microstructures relative to those from Heat I. All Heat II SMAs contain small traces of $Ti_4Ni_2O_x$, TiC, and Ti_2Ni precipitates which are expected in Ti-rich NiTi SMAs [20]. In the 2 at.% Sn sample, Sn appears to segregate at the austenitic grain boundaries to form a channeled web-like structure. From 4 to 6 at.% Sn, Sn appears to act as a nucleation site for austenitic grain boundaries and thus a finer channeled web-like structure is formed. The textured appearance is

caused by slight Sn variation which can be (and was in Heat III) easily dissolved by further solutionization. From 8 to 10 at.% Sn, the NiTi matrix begins to decompose into a TiSn-rich phase of similar chemistry to the lamellar phase (ii, **Fig 3.1b**) present in Heat I alloys.

Fig 3.2 presents the elemental distribution of the NiTi matrix in Heats I and II, as observed with EDS. The Sn content detected in the NiTi matrix increases as a function of nominal Sn concentration, in every alloy besides $Ni_{43.8}Ti_{50.2}Sn_6$. Between the $Ni_{45.8}Ti_{50.2}Sn_4$ and $Ni_{43.8}Ti_{50.2}Sn_6$ alloy, Sn retention in the NiTi matrix decreases from 1.66 to 1.36 at.% Sn. This deviation from the general trend can be attributed to the high abundance of the $Ti_3(Sn,Ni)$ phase observed in the $Ni_{43.8}Ti_{50.2}Sn_6$ microstructure, found in this alloy more so than any other Heat I alloy. Heat II NiTi matrix compositions clearly indicate improved Sn solubility when substituting into Ti lattice sites. At Sn concentrations above 6 at.%, Sn substituted for Ti is retained in the NiTi matrix over three times more effectively than Sn substituted for Ni.

Fig 3.3 shows the transformation temperatures from DSC data from Heat I and II alloys. When Sn is substituted for Ni, alloy transformation temperatures decrease linearly from an A_F of 109°C in the binary $Ni_{49.8}Ti_{50.2}$ control sample to -31°C in the $Ni_{39.8}Ti_{50.2}Sn_{10}$ alloy. Only the 6 at.% Sn alloy deviates from this trend due to poor Sn retention in the NiTi matrix. . The peaks progressively broaden with increasing Sn content which implies Sn prolongs transformation hysteresis in NiTi.

In Heat II, the improved solubility of Sn in the NiTi matrix accounts for a more pronounced shift in transformation temperatures. From $Ni_{49.8}Ti_{50.2}$ to $Ni_{49.8}Ti_{48.2}Sn_2$, A_F decreases substantially from 109°C to 28°C. In the $Ni_{49.8}Ti_{46.2}Sn_4$ alloy, no transformations were observed although they are presumed to occur below -175°C considering the 81°C shift at only 2 at.% Sn. The

transformation peak in the $Ni_{49.8}Ti_{48.2}Sn_2$ alloy is extremely broad and uneven due to the microstructural heterogeneity. To sharpen these transformation peaks and further decrease transformation temperatures, longer solutionization times are necessary, leading to Heat III.

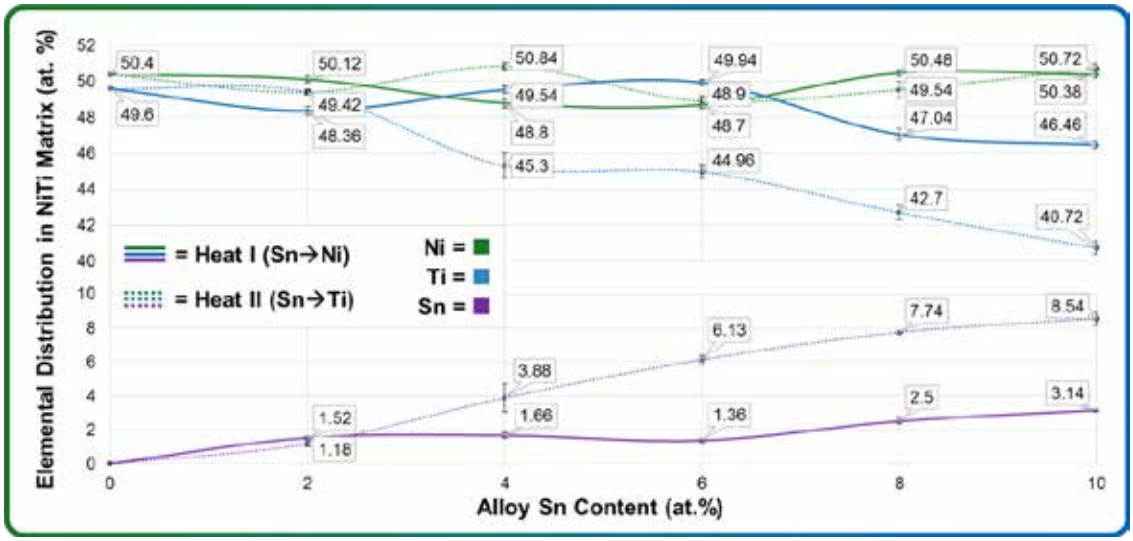

Fig. 3.2. Elemental distribution in the NiTi matrix for NiTiSn SMAs at 2, 4, 6, 8, and 10 at.% Sn, substituting Sn for Ni in Heat I ($Ni_{49.8-x}Ti_{50.2}Sn_x$) and Sn for Ti in Heat II ($Ni_{49.8}Ti_{50.2-x}Sn_x$).

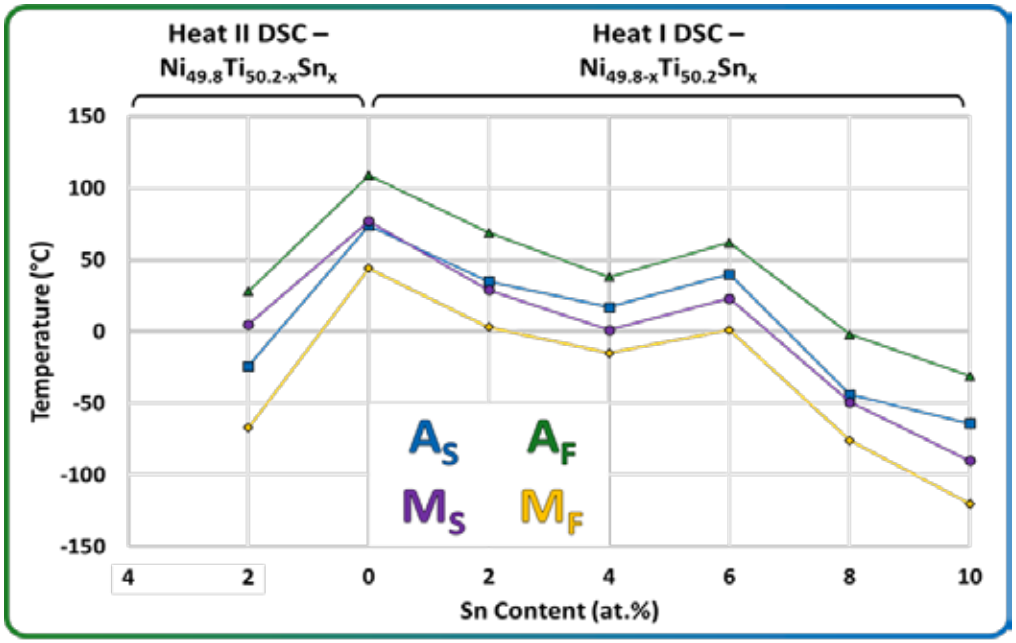

Fig. 3.3. DSC results displaying the transformation temperatures of NiTiSn SMAs from Heat I ($Ni_{49.8-x}Ti_{50.2}Sn_x$) and Heat II ($Ni_{49.8}Ti_{50.2-x}Sn_x$).

3.1.2 Heat III – Effects of Extended Heat Treatments

After determining Sn's preference for Ti lattice sites in NiTi SMAs, the alloys from Heat II, which substitute Sn for Ti, were further solutionized by increasing the heat treatment duration from 30 minutes to 24 hours at 1000°C. As observed in the Heat III microstructures in **Fig 3.1a**, the NiTi matrix is completely uniform up to 4 at.% Sn. From 6 to 8 at.% Sn, slight variation in Sn content is apparent which indicates the need for homogenization by extending heat treatment duration. In the $Ni_{49.8}Ti_{40.2}Sn_{10}$ alloy, the TiSn-rich phase is still present but its faded phase boundaries suggest it may be further dissolved into the NiTi matrix through even longer solutionization times. Due to the extended open-air heat treatments, a higher prevalence of $Ti_2O_x/Ti_4Ni_2O_x$ precipitates are noted, relative to those observed in Heat II alloys.

Fig 3.4 presents the DSC data for Heat III. Since Heat II DSC data indicated no transformations above -175°C in alloys containing 4 to 10 at.% Sn, several additional alloys were produced and characterized in Heat III containing between 2 and 3 at.% Sn content. After extending heat treatment duration, the transformation temperatures of the $Ni_{49.8}Ti_{48.2}Sn_2$ alloy dropped considerably with an A_F shift from 28°C to -32°C. This 60°C decrease can be accounted to the improved Sn retention in the NiTi matrix, which nearly doubled (1.18 at.% à 2.14 at.%), and a higher Ni:Ti ratio due to a larger volume fraction of $Ti_2O_x/Ti_4Ni_2O_x$ precipitates present in the microstructure **(Fig 3.1a).** Based on the DSC results for alloys containing 2.25 to 2.75 at.% Sn, transformation temperatures drop significantly past 2.5 at.% Sn. The $Ni_{49.8}Ti_{47.45}Sn_{2.75}$ alloy exhibited an A_F of -156°C which marks the lowest transformation temperature recorded in this study.

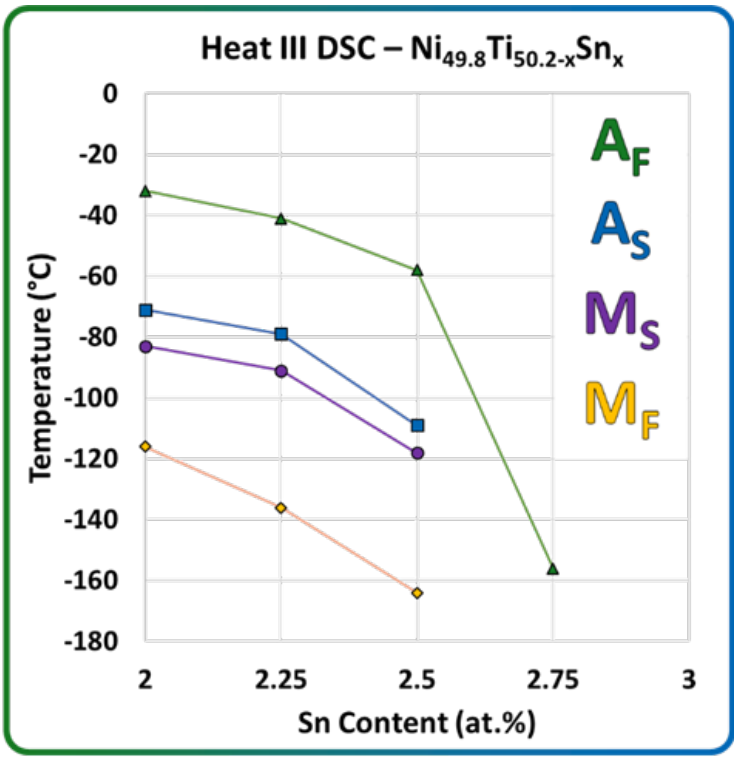

Fig. 3.4. DSC results displaying the transformation temperatures of NiTiSn SMAs from Heat III substituting Sn for Ti ($Ni_{49.8}Ti_{50.2-x}Sn_x$/1000°C for 24 hours).

In Heat III, the transformation plateau in NiTi SMAs was successfully lowered to sub-cryogenic temperatures with less than 3 at.% Sn addition. Additionally, the degree to which this transformation plateau shifts was correlated with respect to Sn additions between 0 and 3 at.%. With the influence of Sn on transformation temperatures sufficiently established for Ti-rich NiTiSn SMAs, Heat IV explored alternative mechanisms for lowering transformation temperatures by increasing the Ni:Ti ratio at fixed Sn contents.

3.1.3 Heats IV-V – Effects of Ni:Ti Ratio and Precipitation Aging

In Heat IV, alloys fixed at 2 and 3 at.% Sn were produced with increasing Ni content between 49.8 and 50.6 at.% Ni. This small Ni increase has been shown to drop transformation temperatures nearly 80°C in binary NiTi [8]. The purpose of Heat IV ($Ni_{49.8+x}Ti_{50.2-x}Sn_3$) was to drive

A_F below the -150°C target temperature to enable their low temperature aging in Heat V. Low temperature aging induces $Ni_4(Ti,Sn)_3$ precipitation which can be used to precisely elevate A_F to -150°C, while simultaneously inducing precipitation strengthening [8, 28, 287, 288].

With regards to the alloy microstructures presented in **Fig 3.5**, $Ti_4Ni_2O_x$, TiC, and Ti_2Ni precipitates were observed with seemingly identical prevalence across all Heat IV alloys. With this considered, the $Ti_4Ni_2O_x$ and TiC precipitates likely formed during the initial arc melting process. Since these precipitates have higher melting temperatures than the parent NiTi matrix, the most practical way of reducing their frequency is by starting with higher purity materials.

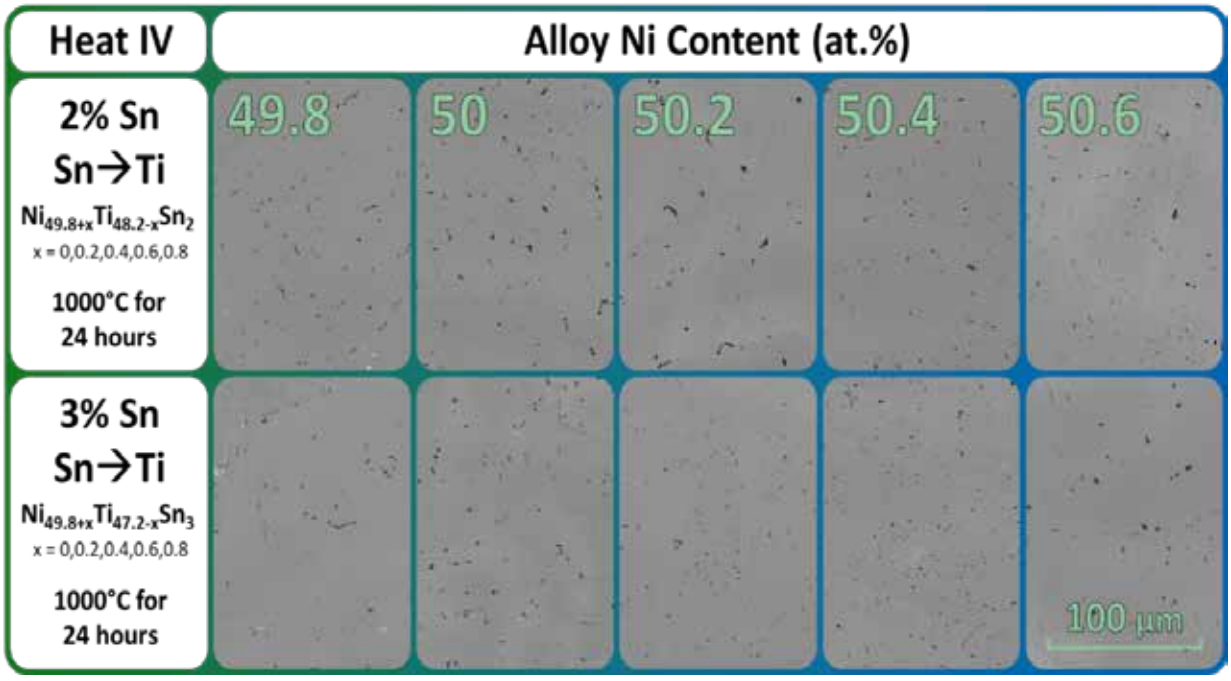

Fig. 3.5. Microstructures of alloys from Heat IV ($Ni_{49.8+x}Ti_{48.2-x}Sn_2$ & $Ni_{49.8+x}Ti_{47.2-x}Sn_3$) where x = 0, 0.2, 0.4, 0.6, and 0.8 at.%.

The DSC results for Heat IV alloys containing 2 at.% Sn are shown in **Fig 3.6**. As expected, transformation temperatures drop significantly as Ni content increases. From 49.8 to 50.2 at.% Ni, A_F drops 56°C (i.e. from -71°C to -127°C) while alloys exceeding 50.2 at.% Ni exhibited no transformations above -175°C.

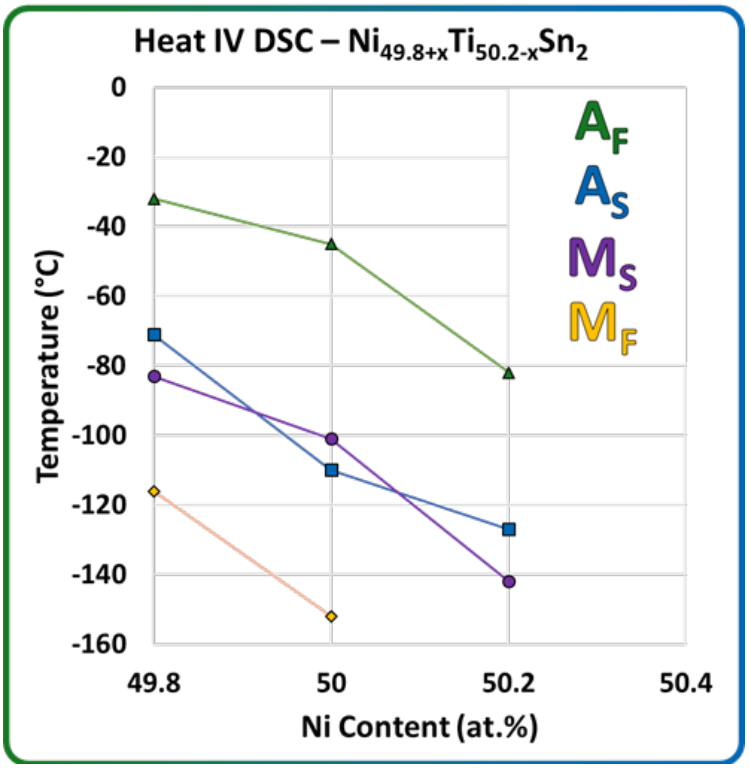

Fig. 3.6. DSC results displaying the transformation temperatures of NiTiSn SMAs from Heat IV ($Ni_{49.8+x}Ti_{48.2-x}Sn_2$/1000°C for 24 hours) where x = 0, 0.2, and 0.4 at.%.

Fig 3.7 shows Vickers hardness data from: a) Heats I-IV as a function of Sn content and b) Heat IV as a function of Ni content. Heat I (Sn à Ni) exhibits much lower hardness relative to Heats II-IV (Sn à Ti) due to the TiSn-rich lamellar phase present in its microstructures. Heats II-III held a relatively constant hardness up to 2 at.% Sn at which point hardness steadily climbed to as high as 579 HV at 10 at.% Sn, suggesting that the lattice strain associated with Sn going into solid solution in the NiTi matrix increases the overall hardness of the SMA. The increasing heterogeneity between the parent matrix and precipitate/lamellar phases at higher Sn concentrations also contributed to the observed hardness increase.

As illustrated in **Figure 3.7b**, alloy hardness decreased with increasing Ni content. The mechanism behind these trends is unclear as hardness is expected to increase as a function of Ni content, due to the higher valency of Ni, which is known to increase the elastic constant, and to

the likelihood of forming precipitates at higher non-stoichiometric concentrations [33]. While all Heat IV SMAs are in the austenitic state, the alloys with 50.6 at.% Ni content are much farther from their respective M_S temperatures and *should* be harder, considering the austenite phase is generally harder than martensite [289]. This atypical relationship between Ni content and hardness in Heat IV alloys should be investigated with higher resolution techniques such as Synchrotron Radiation X-ray Diffraction (SR-XRD) or Transmission Electron Microscopy (TEM) studies for additional insight. Lastly, **Figure 3.7b** also shows the role of increasing Sn content, where the hardness also increases due to an increase in solid solution strengthening and/or precipitation hardening, and this should also be resolved using higher resolution techniques.

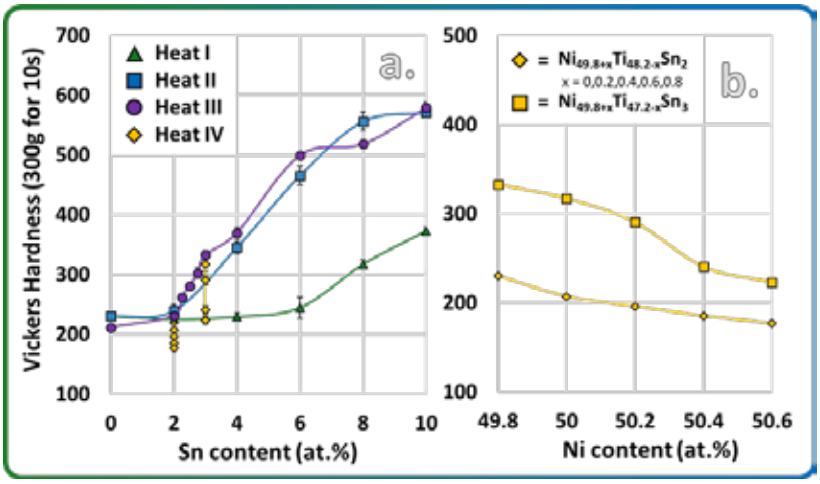

Fig. 3.7. Vickers hardness results for **(a)** Heats I-IV as a function of Sn content, and **(b)** Heat IV as a function of Ni content.

Several precipitation experiments were performed in Heat V with aging temperatures of 500, 550, and 650°C for 12, 24, and 60-hour durations followed by water quenching. Only SMAs containing 50.4 and 50.6 at.% Ni were aged and characterized since these alloys were most inclined to form $Ni_4(Ti,Sn)_3$ precipitates. Several methods were employed to verify the presence of $Ni_4(Ti,Sn)_3$ precipitates. In theory, since $Ni_4(Ti,Sn)_3$ precipitation pulls Ni from the NiTi matrix,

DSC results indicating elevated transformation temperatures in an aged sample would help verify the presence of $Ni_4(Ti,Sn)_3$ precipitates. However, no aged samples displayed any transformations above -175°C so this method for precipitate confirmation was ruled out.

High-resolution SEM imaging near the grain boundaries in aged alloys revealed no signs of nano-precipitation (**Fig 3.8)**. Identifying Ni_4Ti_3 nano-precipitates with high-resolution TEM has been demonstrated [287], and could potentially reveal $Ni_4(Ti,Sn)_3$ precipitation in future studies. With no indication of $Ni_4(Ti,Sn)_3$ precipitation strengthening in Vickers hardness data as well, evidence suggests none of the prescribed aging treatments induced $Ni_4(Ti,Sn)_3$ precipitation.

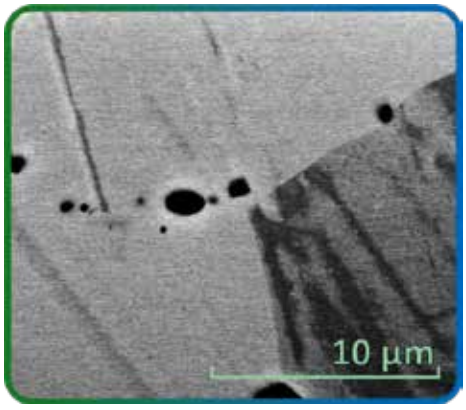

Fig. 3.8. High-resolution SEM image of grain boundaries in a $Ni_{50.6}Ti_{46.4}Sn_3$ SMA solutionized at 1000°C for 24 hours and low temperature aged at 550°C for 24 hours.

3.2 NiTiHf High-Temperature SMAs

The five NiTiHf HTSMA rods hot-rolled in this thesis originate from two Ni-rich melts (FS5 & FS6) with elemental compositions of $Ni_{50.8}Ti_{29.2}Hf_{20}$ and $Ni_{50.7}Ti_{29.4}Hf_{19.9}$, respectively. Two rods from each melt were hot-rolled at 700°C and 800°C, respectively, from an initial diameter of 6.35 mm down to ~1 mm over a series of 25 non-consecutive hot passes. An additional $Ni_{50.7}Ti_{29.4}Hf_{19.9}$ (FS6) HTSMA rod was hot-rolled at 700°C to a ~1 mm final diameter over 50 non-consecutive hot

passes to determine the effects of the reduction rate on the residual strain build up in the material. Since transformation temperatures in Ni-rich NiTi-based SMAs are extremely sensitive to stoichiometric variation [8], the thermomechanical characteristics of NiTiHf rods from different melts will not be directly compared. Instead, a comparison of the two $Ni_{50.8}Ti_{29.2}Hf_{20}$ (FS5) rods is presented first, followed by a comparison of the three $Ni_{50.7}Ti_{29.4}Hf_{19.9}$ (FS6) HTSMA rods.

3.2.1 $Ni_{50.8}Ti_{29.2}Hf_{20}$ HTSMAs

Fig 3.9 displays SEM images of the $Ni_{50.8}Ti_{29.2}Hf_{20}$ (FS5) rods at incremental stages of the hot-rolling process for both rolling temperatures. The microstructure of these HTSMAs is composed of a martensitic matrix permeated by dark secondary phase particles identified as $Ti_4Ni_2O_x$. At both rolling temperatures the average size of the martensitic grains decreases linearly, from ~21 µm in the 5th pass, to ~7 µm after undergoing 25 hot passes to a 97.5% reduction in cross-sectional area.

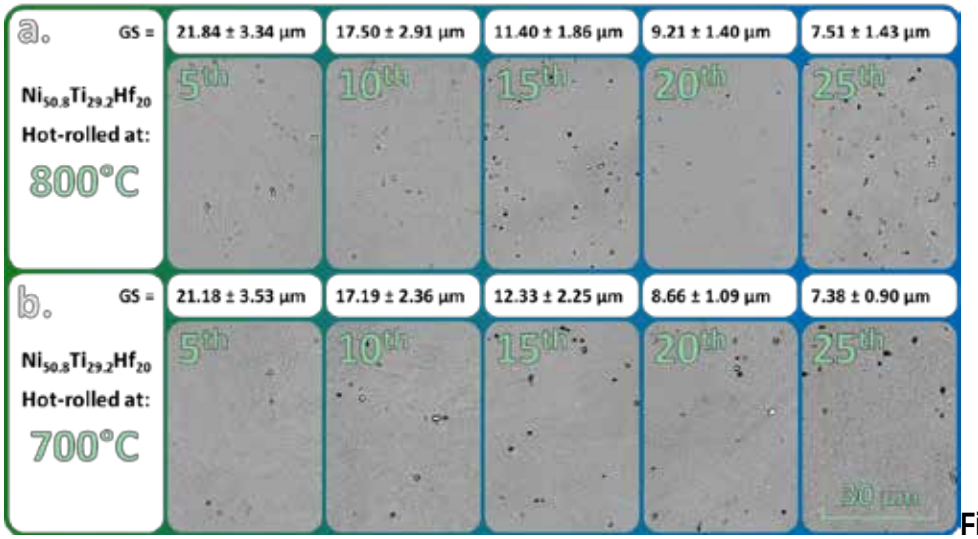

Fig. 3.9. Microstructures and grain size measurements for $Ni_{50.8}Ti_{29.2}Hf_{20}$ HTSMA rods hot-rolled at a) 800°C, and b) 700°C for the five documented stages of the hot-rolling process.

The DSC results, indicating the transformation temperatures of the $Ni_{50.8}Ti_{29.2}Hf_{20}$ rods hot-rolled at 800°C and 700°C are displayed in **Fig 3.10a** and **Fig 3.10b**, respectively. In the rod hot-rolled at 800°C, transformation temperatures remain stable while transformation hysteresis progressively widens in each subsequent pass. In the rod hot-rolled at 700°C, transformation temperatures increase significantly by the 5th pass with a change in A_F of ~138°C (101°C à 239°C). In the following passes (10th-25th), transformation temperatures decrease and stabilize by the 25th pass at an A_F of 187°C.

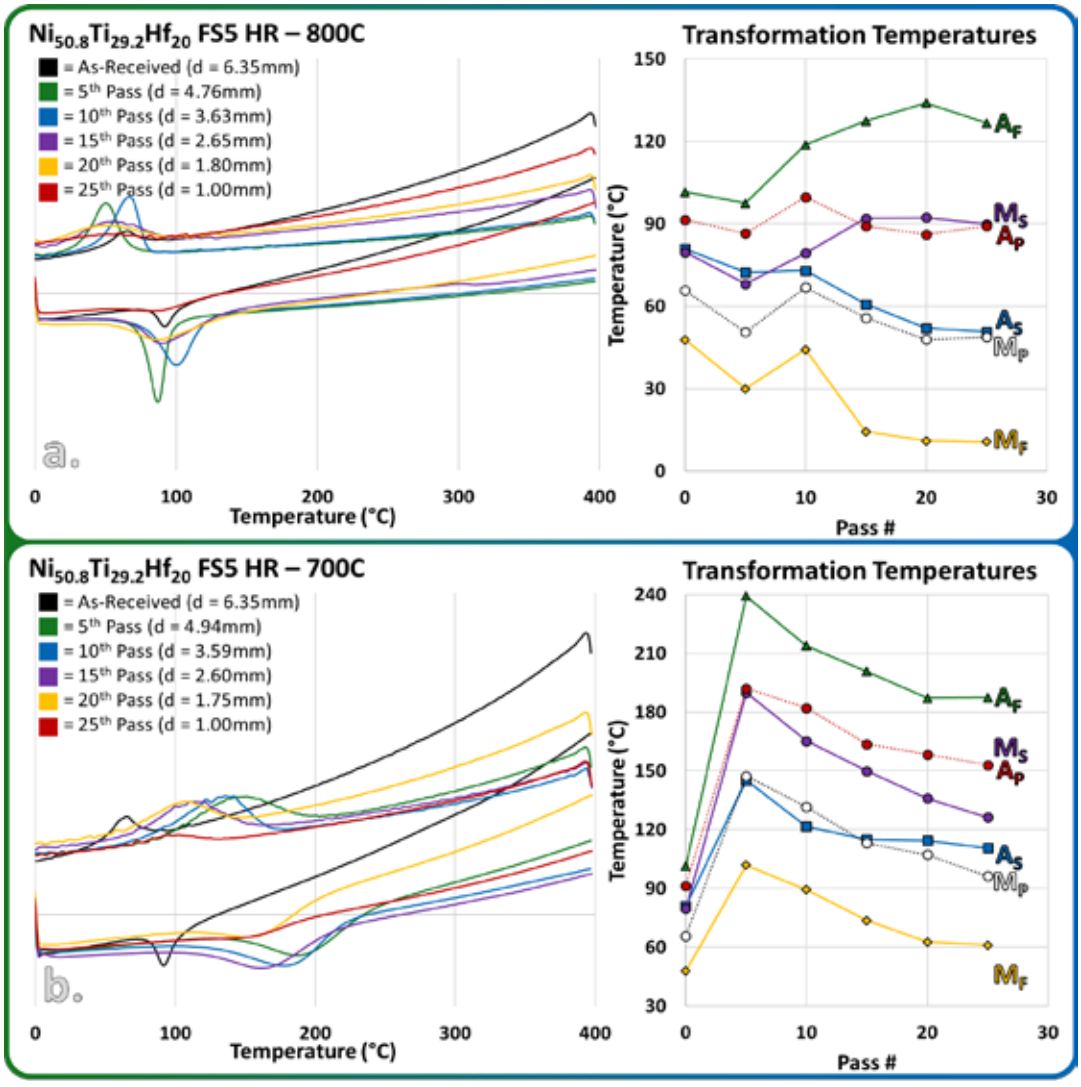

Fig. 3.10. DSC results displaying the transformation temperatures of $Ni_{50.8}Ti_{29.2}Hf_{20}$ HTSMA rods hot-rolled at a) 800°C, and b) 700°C for the five recorded stages of the hot-rolling process.

Fig 3.11 displays the transformation peaks (A_P/M_P) and average martensitic grain size for both $Ni_{50.8}Ti_{29.2}Hf_{20}$ HTSMA rods as a function of the cross-sectional area-reduction of the rod/wire. In the rod hot-rolled at 700°C, the substantial increase in transformation temperatures observed in the 5th pass can be attributed to H-phase nano-precipitation. These H-phase precipitates, formed during the initial 30-minute heating to 700°C, pulled Ni from the matrix consequently raising transformation temperatures. Once the material was saturated with H-phase precipitates, transformation temperatures began to decrease in subsequent passes (10th-25th) due to residual strain buildup. This permanent strain was also caused by H-phase precipitation since the H-phase does not exhibit any shape memory characteristics. In the rod hot-rolled at 800°C, transformation temperatures remained relatively stable across all 5 documented samples. This stability is due to the absence of H-phase precipitates, which were dissolutionized into the matrix at this rolling temperature (800°C). The similar rates of grain refinement observed in both $Ni_{50.8}Ti_{29.2}Hf_{20}$ rods indicate rolling temperatures have no significant effect on martensitic grain size.

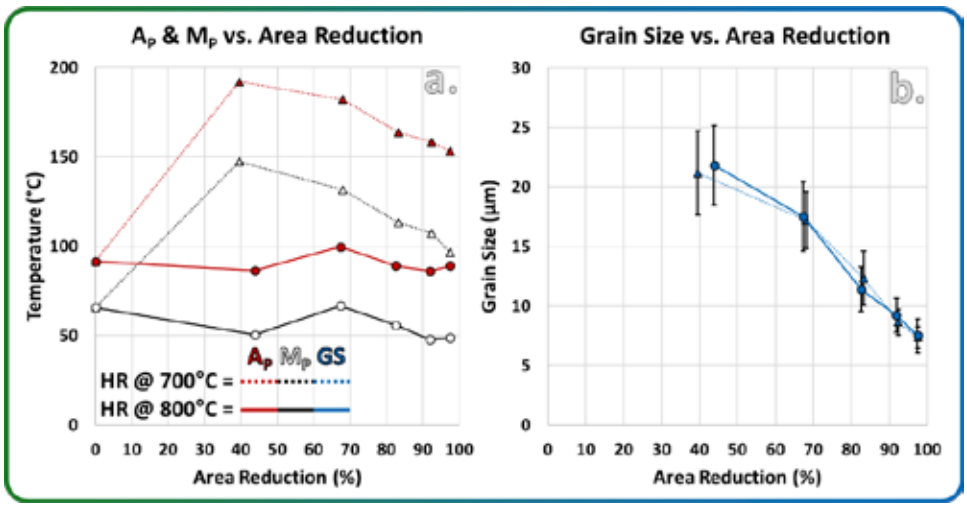

Fig. 3.11. A comparison between the a) transformation peaks (A_P/M_P), and b) grain size evolution of the $Ni_{50.8}Ti_{29.2}Hf_{20}$ HTSMA rods hot-rolled at 700°C and 800°C as a function of the cross-sectional area-reduction of the rod/wire.

3.2.2 $Ni_{50.7}Ti_{29.4}Hf_{19.9}$ HTSMAs

The microstructures for the three $Ni_{50.7}Ti_{29.4}Hf_{19.9}$ (FS6) HTSMA rods are shown in **Fig 3.12**. The martensitic matrix and darker $Ti_4Ni_2O_x$ precipitate morphology closely resemble the microstructures of the two $Ni_{50.8}Ti_{29.2}Hf_{20}$ (FS5) rods discussed previously. The average martensitic grain size reduces as a function of the cross-sectional area-reduction of the wire across all three $Ni_{50.7}Ti_{29.4}Hf_{19.9}$ HTSMA rods.

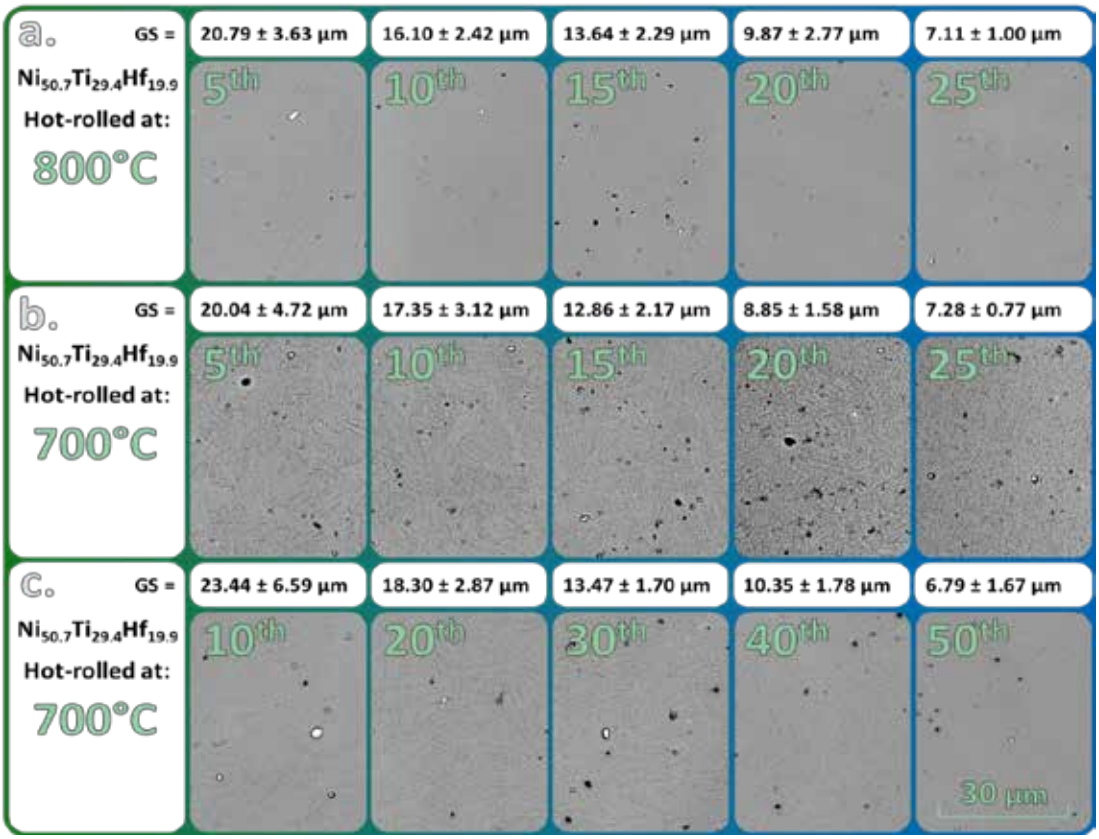

Fig. 3.12. Microstructures and grain size measurements for $Ni_{50.7}Ti_{29.4}Hf_{19.9}$ HTSMA rods hot-rolled at a) 800°C for 25 passes, b) 700°C for 25 passes, and c) 700°C for 50 passes for the five documented stages of the hot-rolling process.

Fig 3.13 displays a cross-sectional view of the enveloping oxide layers on each $Ni_{50.7}Ti_{29.4}Hf_{19.9}$ HTSMA rod at various stages of the hot-rolling process. In the first documented hot pass of all three rods, both the oxide thickness and prevalence of surface cracking are comparable. By

the second recorded hot pass stage, the oxide thickens and begins diffusing into the bulk material through exposed surface cracks.

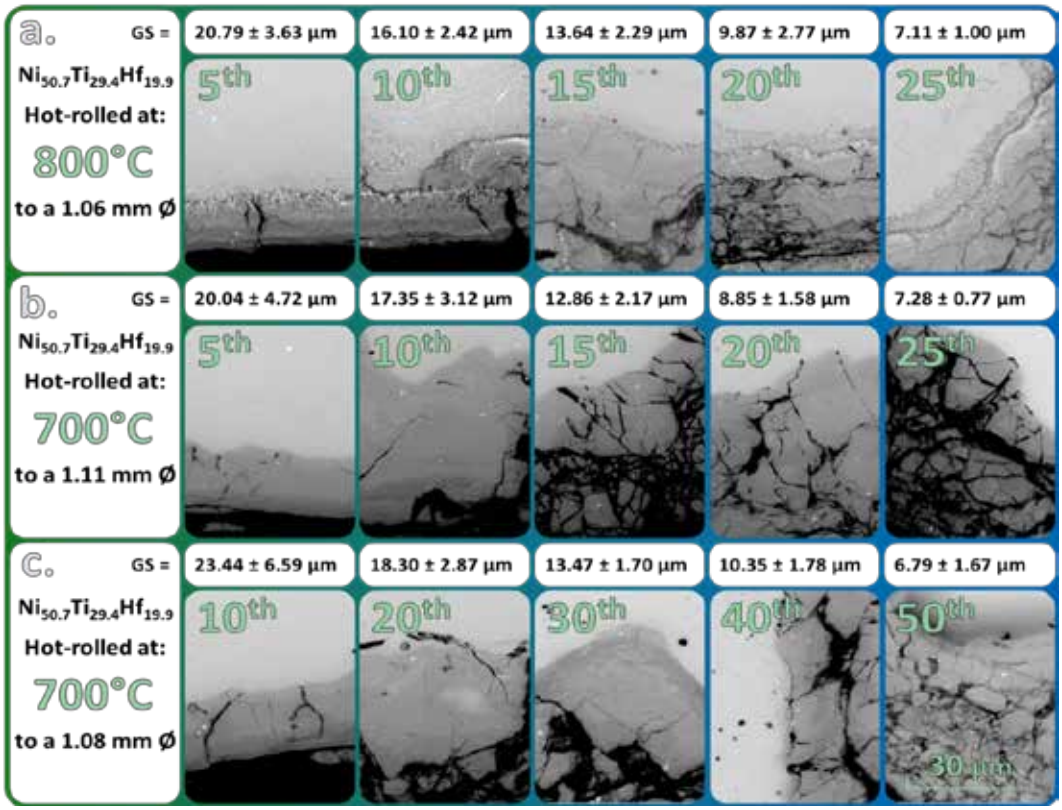

Fig. 3.13. SEM images of the oxide layer morphology in $Ni_{50.7}Ti_{29.4}Hf_{19.9}$ HTSMA rods hot-rolled at a) 800°C for 25 passes, b) 700°C for 25 passes, and c) 700°C for 50 passes for the five documented stages of the hot-rolling process.

In the third documented stage, the oxide begins to lose coherency with the bulk matrix. This causes the oxide to flake off during subsequent hot passes, re-exposing the bulk material for new oxide layers to form. Due to this mechanism, the oxide morphology of the fourth and fifth stages (20^{th}/25^{th} or 40^{th}/50^{th} pass) does not offer any additional insight as they appear analogous to that of previous stages.

Along the oxide interior of the rod hot-rolled at 800°C, a fine needle-like structure is noted. This pre-oxide feature does not appear in either of the rods hot-rolled at 700°C, offering a primary distinction between the oxide morphologies of both rolling temperatures. To further

investigate this distinction, a compositional gradient of the oxide at both rolling temperatures was measured with EDS line spectra, shown in **Fig 3.14**. These results indicate the white needle-like structure exhibits a Hf-rich, Ni-lean composition with respect to the bulk stoichiometry, similar to that observed in Carl et al. [281].

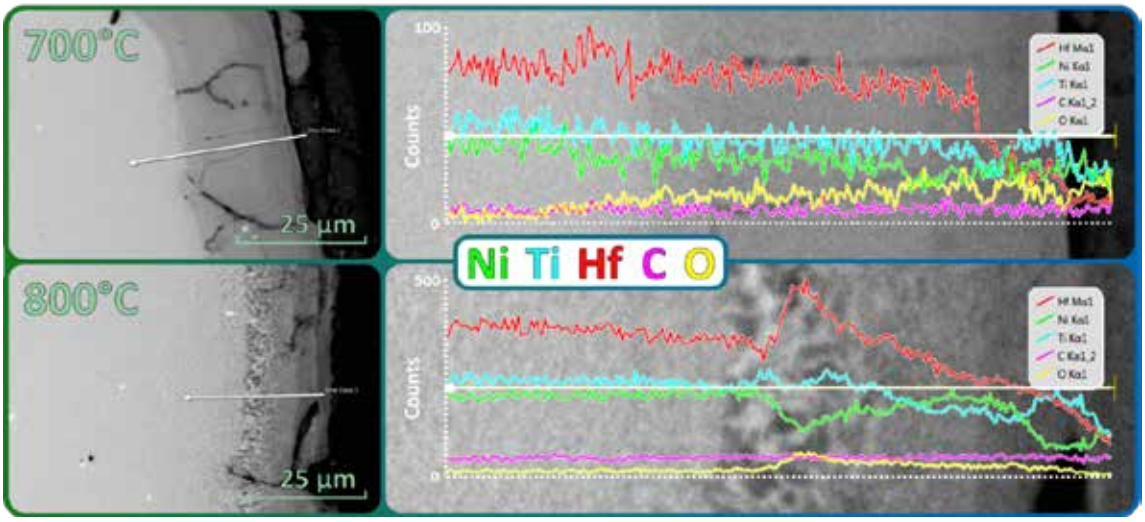

Fig. 3.14. EDS line spectra displaying the distribution of Ni, Ti, Hf, C, and O across the oxide layers of $Ni_{50.7}Ti_{29.4}Hf_{19.9}$ HTSMA rods after 5 hot passes at 700°C or 800°C.

The DSC results shown in **Fig 3.15** reveal the transformation behaviors of the $Ni_{50.7}Ti_{29.4}Hf_{19.9}$ HTSMA rods hot-rolled at a) 800°C for 25 passes, b) 700°C for 25 passes, and c) 700°C for 50 passes, respectively. In the rod hot-rolled at 800°C, the stability of A_P and M_P signify no significant shifts in transformation temperatures across all hot-rolling stages. In the rod hot-rolled at 700°C for 25 hot passes, transformation temperatures steadily rise, peaking in the 10th pass, and progressively falling throughout the remaining stages. These trends were paralleled by the rod hot-rolled at 700°C for 50 passes, which experienced an A_F increase of ~95°C by the 20th pass (170°C à 265°C), before dropping to 192°C in the 50th and final pass.

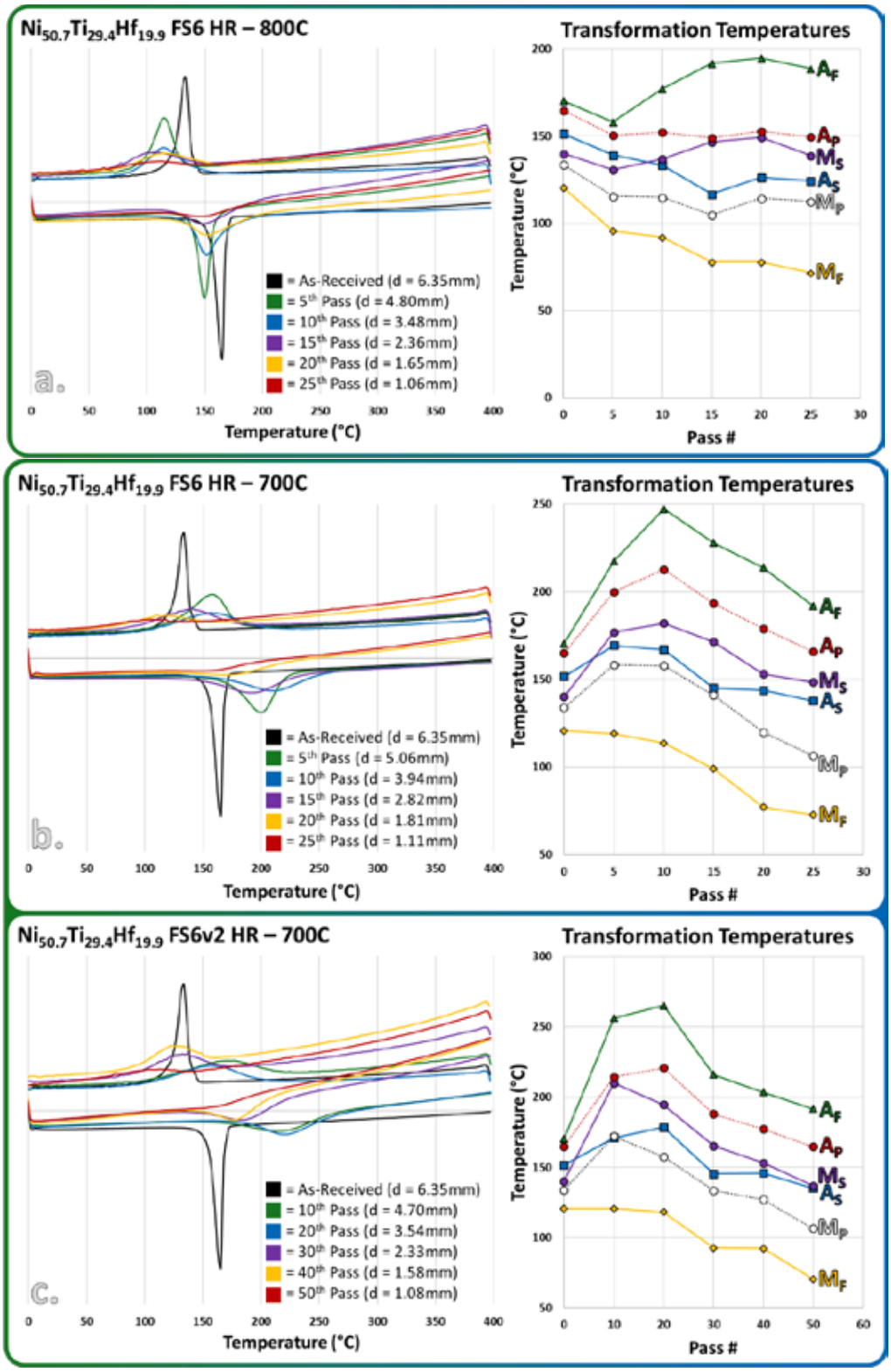

Fig. 3.15. DSC results displaying the transformation temperatures of $Ni_{50.7}Ti_{29.4}Hf_{19.9}$ HTSMA rods hot-rolled at a) 800°C for 25 passes, b) 700°C for 25 passes, and c) 700°C for 50 passes for the five recorded stages of the hot-rolling process.

Fig 3.16 displays the transformation peaks (A_P/M_P) and average martensitic grain size for the three $Ni_{50.7}Ti_{29.4}Hf_{19.9}$ HTSMA rods as a function of the cross-sectional area-reduction of the rod/wire. Across the five documented hot-rolling stages, grain refinement is noted in all three $Ni_{50.7}Ti_{29.4}Hf_{19.9}$ rods. In the first two stages, the martensitic grains in the rod rolled at 700°C for 50 passes appear slightly larger than grains in the other two rods; however, due to high variability in the grain size measurements, no effects of rolling temperature on grain size can be confirmed.

In both rods hot-rolled at 700°C, the initial increase in transformation temperatures observed in the 5th & 10th pass was caused by H-phase nano-precipitation, as discussed with the $Ni_{50.8}Ti_{29.2}Hf_{20}$ (FS5) rods. The rod hot-rolled at 700°C for 50 passes exhibits slightly higher transformation temperatures than the 25-pass counterpart, due to the additional thermal hold time. In other words, since each rod spends 5 minutes in the furnace after each pass, the rod that underwent 50 passes was kept at 700°C for twice as long, likely precipitating slightly more H-phase as a result. Aside from this small deviation, the transformation temperatures of the rods hot-rolled at 700°C were nearly identical, thus validating the accuracy of the results.

In the rod hot-rolled at 800°C, transformation temperatures remained relatively stable across all 5 documented stages, although a minor decrease is still noted. This stability is due to the absence of H-phase precipitates, which were dissolutionized into the matrix at this rolling temperature (800°C). The Hf-rich needles located in the pre-oxide layer of this $Ni_{50.7}Ti_{29.4}Hf_{19.9}$ HTSMA rod are detrimental to further thermomechanical processing. This Hf-rich oxide is removed from the material with each pass, due to the incoherency of the oxide/matrix interface noted by the 15th pass. The depletion of Hf through oxide delamination will progressively and

exponentially lower transformation temperatures the further the wire is reduced, due to the increasing volume fraction of the oxide/wire [283].

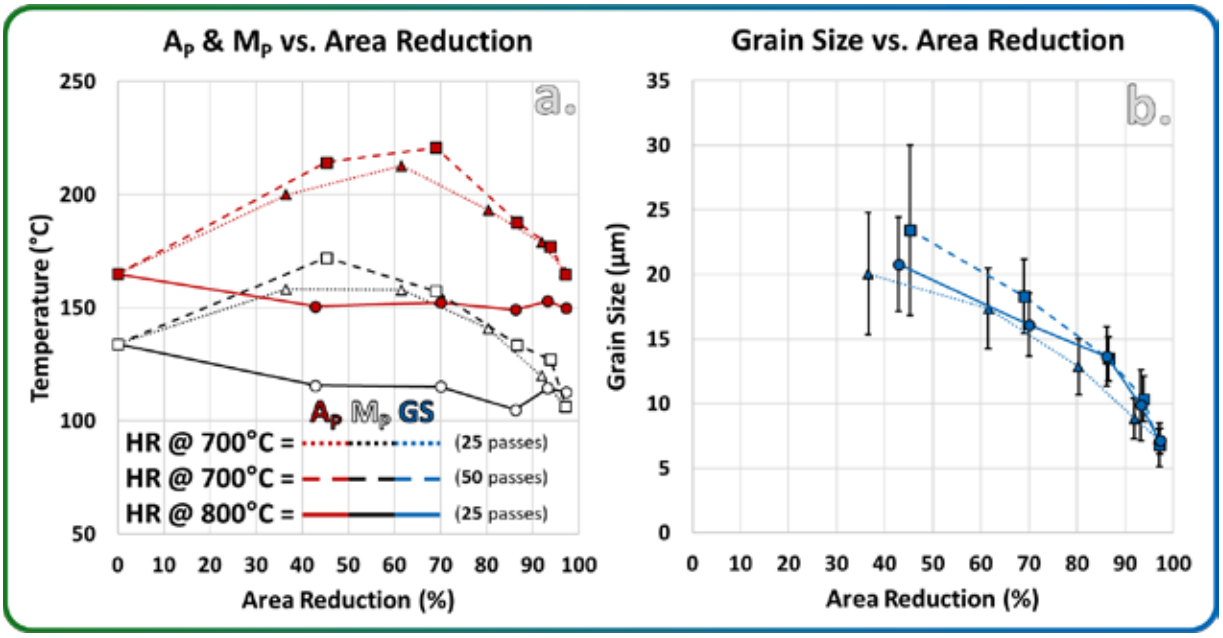

Fig. 3.16. A comparison between the a) transformation peaks (A_P/M_P), and b) grain size evolution of the $Ni_{50.7}Ti_{29.4}Hf_{19.9}$ HTSMA rods hot-rolled at 800°C for 25 passes, 700°C for 25 passes, and 700°C for 50 passes as a function of the cross-sectional area-reduction of the rod/wire.

CHAPTER 4

CONCLUSIONS AND FUTURE RESEARCH

4.1 NiTiSn Low-Temperature SMAs

The viability of NiTiSn SMAs in low-temperature actuator applications was investigated over a series of five alloy heats (Heats I-V). First, the site preference of Sn in near-equiatomic NiTi was evaluated by substituting Sn for Ni in Heat I ($Ni_{49.8-x}Ti_{50.2}Sn_x$), and Sn for Ti in Heat II ($Ni_{49.8}Ti_{50.2-x}Sn_x$ where x = 2, 4, 6, 8, and 10 at.%). Results confirmed Sn substitutes into Ti lattice sites rather than Ni sites in near equiatomic NiTi due to a more similar electronic configuration. Both Sn and Ti prefer to give away two electrons to reach a lower energy full shell state, specifically $4d^{10}$ and $4s^2$ respectively, while Ni prefers to gain two electrons.

After determining Sn's preference for Ti lattice sites in NiTi SMAs, alloys substituting Sn for Ti ($Ni_{49.8-x}Ti_{50.2}Sn_x$ where x = 2, 2.25, 2.5, 2.75, 3, 4, 6, 8, and 10 at.%) were produced and solution annealed. In this heat (Heat III), the cryogenic transformation capabilities of the NiTiSn SMA system were successfully demonstrated in NiTiSn SMAs with less than 3 at.% Sn addition. Additionally, the effects of Sn addition on transformation temperatures in near-equiatomic NiTi was quantitatively correlated up to 3 at.% Sn.

With the influence of Sn on transformation temperatures sufficiently established for Ti-rich NiTiSn SMAs, Heat IV explored alternative mechanisms for lowering transformation temperatures by increasing the Ni:Ti ratio at a fixed Sn content ($Ni_{49.8+x}Ti_{48.2-x}Sn_2$ where x = 0, 0.2, 0.4, 0.6, and 0.8 at.%). NiTiSn LTSMAs with Ni content exceeding 50.2 at.% were shown to exhibit sub-cryogenic transformation temperatures (<-175°C).

In Heat V, Ni-rich NiTiSn LTSMAs were low-temperature aged in an effort to promote the formation of $Ni_4(Ti,Sn)_3$ precipitates which aid in fine-tuning transformation temperatures [287], strengthen the alloy, and improve transformation behaviors. None of the aging techniques employed in this thesis successfully induced $Ni_4(Ti,Sn)_3$ precipitation, although a promising new aging technique is presented in Section 4.3.

4.2 NiTiHf High-Temperature SMAs

The thermomechanical processability of NiTiHf HTSMA wires was investigated in an effort to optimize the rolling/drawing process for NiTiHf HTSMAs. Five Ni-rich NiTiHf HTSMA rods ($Ni_{50.8}Ti_{29.2}Hf_{20}$ & $Ni_{50.7}Ti_{29.4}Hf_{19.9}$) were hot-rolled to a ~97% reduction in cross-sectional area over the course of 25 or 50 non-consecutive hot passes at either 700°C or 800°C. The evolution of various microstructural features (grain size reduction, oxide growth, and nano-precipitation) were observed at incremental stages of the hot rolling process and linked to the thermal and mechanical responses of respective HTSMA rods/wires.

The average martensitic grain size decreased linearly as a function of the cross-sectional area-reduction of the rod/wire across all five NiTiHf HTSMAs. Rolling temperature (700°C vs. 800°C) and/or composition ($Ni_{50.8}Ti_{29.2}Hf_{20}$ vs. $Ni_{50.7}Ti_{29.4}Hf_{19.9}$) showed no observable influence on grain size.

The $Ni_{50.8}Ti_{29.2}Hf_{20}$ and $Ni_{50.7}Ti_{29.4}Hf_{19.9}$ HTSMAs exhibited stable transformation temperatures when hot-rolled at 800°C; however, a Hf-rich needle-like structure observed in the oxide morphology poses concerns for further thermomechanical processing. As the volume fraction of the oxide/wire increases with each pass, more Hf will be removed from the material

through oxide delamination, progressively and exponentially lowering transformation temperatures the further the wire is reduced.

The detrimental Hf-rich oxide was not observed in the NiTiHf HTSMAs hot-rolled at 700°C; however, at this rolling temperature, transformation temperatures were increased substantially in the first 5 hot passes due to H-phase nano-precipitation. These H-phase precipitates, formed during the initial 30-minute heating to 700°C, pulled Ni from the parent matrix, consequently raising the transformation temperatures. Once the material was saturated with H-phase precipitates, transformation temperatures began to decrease in subsequent passes (10^{th}-25^{th}) due to residual strain buildup. This permanent strain was also caused by H-phase precipitation, since the H-phase does not exhibit any shape memory characteristics.

4.3 Future Research

In a final attempt to demonstrate $Ni_4(Ti,Sn)_3$ precipitation, a $Ni_{50.8}Ti_{48.2}Sn_1$ alloy was melted, homogenized, and cold rolled to ~70%. The alloy was aged at 550, 650, 750, and 850°C, respectively, followed by a furnace cooling. The alternative cooling technique, high Ni content (50.8 at.% in this case), and point defects generated from cold-work are all thought to promote $Ni_4(Ti,Sn)_3$ precipitation. The phases present in these samples are currently being determined using Synchrotron Radiation X-ray Diffraction (SR-XRD) experiments. An additional in-situ SR-XRD experiment (700°C at 5°C/min) on an un-aged $Ni_{50.8}Ti_{48.2}Sn_1$ sample will be performed to reveal precisely when $Ni_4(Ti,Sn)_3$ precipitation occurs. Aside from precipitation studies, the mechanical properties and processability of NiTiSn LTSMAs will be assessed through cryogenic compression testing and hot rolling studies, respectively.

Strain recovery testing on the five NiTiHf HTSMA rods hot-rolled in this thesis will be performed shortly to observe how H-phase precipitates affect the thermomechanical behaviors. The NiTiHf wires will be further drawn (1 mm à 250 µm) using a new hot-drawing technique that mitigates several known issues with cold-drawing NiTiHf [283].

REFERENCES

1. Duerig, T., A. Pelton, and D. Stöckel, *An overview of nitinol medical applications.* Materials Science and Engineering: A, 1999. **273**: p. 149-160.

2. Otsuka, K. and X. Ren, *Physical metallurgy of Ti–Ni-based shape memory alloys.* Progress in materials science, 2005. **50**(5): p. 511-678.

3. Benafan, O., et al., *Shape memory alloy actuator design: CASMART collaborative best practices and case studies.* International Journal of Mechanics and Materials in Design, 2014. **10**(1): p. 1-42.

4. Ma, J., I. Karaman, and R.D. Noebe, *High temperature shape memory alloys.* International Materials Reviews, 2010. **55**(5): p. 257-315.

5. Van Humbeeck, J., *Non-medical applications of shape memory alloys.* Materials Science and Engineering: A, 1999. **273**: p. 134-148.

6. Barbarino, S., et al., *A review on shape memory alloys with applications to morphing aircraft.* Smart Materials and Structures, 2014. **23**(6): p. 063001.

7. Mohd Jani, J., et al., *A review of shape memory alloy research, applications and opportunities.* Materials & Design (1980-2015), 2014. **56**: p. 1078-1113.

8. Frenzel, J., et al., *Influence of Ni on martensitic phase transformations in NiTi shape memory alloys.* Acta Materialia, 2010. **58**(9): p. 3444-3458.

9. Frenzel, J., et al., *On the effect of alloy composition on martensite start temperatures and latent heats in Ni–Ti-based shape memory alloys.* Acta Materialia, 2015. **90**: p. 213-231.

10. Rios, O., et al. *Characterization of Ternary NiTiPt High-Temperature Shape Memory Alloys*. in *International Society for Optical Engineering*. 2005.

11. Krishnan, V., *Low Temperature Nitife Shape Memory Alloys: Actuator Engineering And Investigation Of Deformation Mechanisms Using In Situ Neutr.* 2007.

12. Wheeler, R.W., et al. *Engineering Design Tools for Shape Memory Alloy Actuators: CASMART Collaborative Best Practices and Case Studies*. in *ASME 2016 Conference on Smart Materials, Adaptive Structures and Intelligent Systems*. 2016. American Society of Mechanical Engineers.

13. Kumar, P. and D. Lagoudas, *Introduction to shape memory alloys*, in *Shape memory alloys*. 2008, Springer. p. 1-51.

14. Kurdjumov, G. and L. Khandros, Doklady Akad. Nauk S.S.S.R., 1949. **56**.

15. Buehler, W.J., J. Gilfrich, and R. Wiley, *Effect of low-temperature phase changes on the mechanical properties of alloys near composition TiNi.* Journal of applied physics, 1963. **34**(5): p. 1475-1477.

16. Hanlon, J., S. Butler, and R. Wasilewski, *Effect of martensitic transformation on the electrical and magnetic properties of NiTi.* Transactions of the Metallurgical Society of AIME, 1967. **239**(9): p. 1323-1326.

17. Purdy, G.R. and J.G. Parr, *A study of the Titanium-Nickel System Between Ti2Ni and TiNi.* Transactions of the Metallurgical Society of AIME, 1960.

18. Wang, F.E., W.J. Buehler, and S.J. Pickart, *Crystal Structure and a Unique``Martensitic''Transition of TiNi.* Journal of Applied Physics, 1965. **36**(10): p. 3232-3239.

19. Wasilewski, R., S. Butler, and J. Hanlon, *On the martensitic transformation in TiNi.* Metal Science Journal, 1967. **1**(1): p. 104-110.

20. Frenzel, J., et al., *Influence of carbon on martensitic phase transformations in NiTi shape memory alloys.* Acta Materialia, 2007. **55**(4): p. 1331-1341.

21. Khalil-Allafi, J., A. Dlouhy, and G. Eggeler, *Ni4Ti3-precipitation during aging of NiTi shape memory alloys and its influence on martensitic phase transformations.* Acta Materialia, 2002. **50**(17): p. 4255-4274.

22. Lin, H., et al., *The effects of cold rolling on the martensitic transformation of an equiatomic TiNi alloy.* Acta metallurgica et materialia, 1991. **39**(9): p. 2069-2080.

23. Olson, G.B. and M. Cohen, *Thermoelastic behavior in martensitic transformations.* Scripta Metallurgica, 1975. **9**(11): p. 1247-1254.

24. Otubo, J., et al., *The influence of carbon and oxygen content on the martensitic transformation temperatures and enthalpies of NiTi shape memory alloy.* Materials Science and Engineering: A, 2008. **481-482**: p. 639-642.

25. Piao, M., et al., *Mechanism of the As temperature increase by pre-deformation in thermoelastic alloys.* Materials Transactions, JIM, 1993. **34**(10): p. 919-929.

26. Shi, X., et al., *Grain size effect on the martensitic transformation temperatures of nanocrystalline NiTi alloy.* Smart Materials and Structures, 2015. **24**(7): p. 072001.

27. Świec, P., et al., *Structure and Properties of NiTi Shape Memory Alloy after Cold Rolling in Martensitic State.* Acta Physica Polonica A, 2016. **130**(4): p. 1081-1084.

28. Young, M.L., et al., *Nanoindentation of pseudoelastic NiTi containing Ni4Ti3 precipitates.* International Journal of Materials Research, 2012. **103**(12): p. 1434-1439.

29. Massalski, T.B., et al., *Binary Alloy Phase Diagrams*. 2nd ed. Vol. 3. 1990, Materials Park, Ohio, USA: ASM International.

30. Wang, F. *The Mechanical Properties as a Function of Temperature and Free Electron Concentration in Stoichiometric TiXi, TiCo and TiFe Alloys*. in *ICF1, Japan 1965*. 1966.

31. Eckelmeyer, K., *The effect of alloying on the shape memory phenomenon in nitinol.* Scripta Metallurgica, 1976. **10**(8): p. 667-672.

32. Melton, K.N. and O. Mercier, *The effect of opposing stress on shape memory and martensitic reversion.* Scripta Metallurgica, 1978. **12**(1): p. 5-9.

33. Zarinejad, M. and Y. Liu, *Dependence of Transformation Temperatures of NiTi-based Shape-Memory Alloys on the Number and Concentration of Valence Electrons.* Advanced Functional Materials, 2008. **18**(18): p. 2789-2794.

34. Gilman, J.J., R.W. Cumberland, and R.B. Kaner, *Design of hard crystals.* International Journal of Refractory Metals and Hard Materials, 2006. **24**(1): p. 1-5.

35. Singh, N., et al., *Effect of ternary additions to structural properties of NiTi alloys.* Computational Materials Science, 2016. **112, Part A**: p. 347-355.

36. Zheng, Y., et al., *Microstructure and phase transformation of TiNi alloy with addition of third element Sn.* Rare Metal Materials and Engineering 2004. **33**(6): p. 215-217.

37. Kim, J.-h., et al., *Microstructures and martensitic transformation behavior of Ti–Ni–Sn alloys.* Scripta Materialia, 2011. **65**(7): p. 608-610.

38. Kim, J.-h., et al., *Crystallization and martensitic transformation behavior of Ti–Ni–Sn alloy ribbons.* Intermetallics, 2012. **30**: p. 51-56.

39. Choi, H.-j., et al., *Crystallization behavior and microstructure of Ti–36Ni–7Sn (at.%) alloy ribbons.* Scripta Materialia, 2011. **65**(7): p. 611-614.

40. Choe, H.-j., et al., *Microstructure and martensitic transformation behavior of crystallized Ti–36Ni–7Sn (at%) alloy ribbons.* Journal of Alloys and Compounds, 2013. **577**: p. S195-S199.

41. Tong, Y., et al., *Two-way shape memory effect of TiNiSn alloys developed by martensitic deformation.* Materials Science and Engineering: A, 2012. **550**: p. 434-437.

42. Kim, J.-h., et al., *Martensitic transformation behavior of Ti–Ni–Sn alloys.* Journal of Alloys and Compounds, 2013. **577**: p. S200-S204.

43. Jang, J.-y., et al., *Martensitic transformation behavior in Ti–Ni–X (Ag, In, Sn, Sb, Te, Tl, Pb, Bi) ternary alloys.* Materials Research Bulletin, 2013. **48**(12): p. 5064-5069.

44. Douglas, J.E., et al., *Phase stability and property evolution of biphasic Ti–Ni–Sn alloys for use in thermoelectric applications.* Journal of Applied Physics, 2014. **115**(4): p. 043720.

45. Lu, B.-c. and J. Xu, *Glass formation of Ti–Ni–Sn ternary alloys correlated with TiNi–Ti 3 Sn pseudo binary eutectics.* Journal of Non-Crystalline Solids, 2008. **354**(52): p. 5425-5431.

46. Romaka, V., et al., *Phase equilibria, formation, crystal and electronic structure of ternary compounds in Ti–Ni–Sn and Ti–Ni–Sb ternary systems.* Journal of Solid State Chemistry, 2013. **197**: p. 103-112.

47. Abujudom, D.N., et al., *High transformation temperature shape memory alloy*. 1992. p. 1-10.

48. Beyer, J. and J.H. Mulder. *Recent developments in high temperature shape memory alloys*. in *Materials Research Society*. 1994.

49. Han, X.D., Z. Zhang, and T. Li. *The studies of the microstructure and the martensite transformations in a Ti36.5Ni48.5Hf15 alloy*. in *International Symposium on Shape Memory Materials*. 1994. Beijing China.

50. Kolomytsev, V.I., *The effect of alloying by 3d, 4d, 5d transition metal klements on martensite transformation temperatures in compound TiNi.* Scripta Metallurgica et Materialia, 1994. **31**(10): p. 1415-1420.

51. Mulder, J.H., et al. *On the High Temperature Shape Memory Capabilities of Ni-(TiZr) and Ni-(TiHf) Alloys*. in *Shape Memory and Superelastic Technologies*. 1994. Pacific Grove California.

52. Pu, Z., H. Tseng, and K. Wu. *An innovative system of high temperature shape memory alloys*. in *International Society for Optical Engineering*. 1994.

53. Pu, Z., K. Wu, and Y. Liu. *Structure and Properties of NiTi-Hf Rapidly Solidified High Temperature Shape Memory Alloys*. in *International Symposium on Shape Memory Materials*. 1994. Beijing China.

54. Russell, S.M. and F. Sczerzenie. *Engineering Considerations in the Application of NiTiHf and NiAI as Practical High-Temperature Shape Memory Alloys*. in *Materials Research Society*. 1994. Cambridge University Press.

55. Tuominen, S.M. *High Transformation Temperature Ni-Ti-Hf Alloys*. in *Shape Memory and Superelastic Technologies*. 1994. Pacific Grove California.

56. Zhu, Y., et al. *The Stability of NiTi-Pd and NiTi-Hf High Temperature Shape Memory Alloys*. in *International Symposium on Shape Memory Materials*. 1994. Beijing China.

57. Angst, D., P. Thoma, and M. Kao. *The Effect of Hafnium Content on the Transformation Temperatures of Ni49Ti51-xHfx. Shape Memory Alloys*. in *Journal de Physique IV*. 1995.

58. Han, S., et al., *The studies of the martensite transformations in a Ti36.5Ni48.5Hf15 alloy.* Scripta Metallurgica et Materialia, 1995. **32**(9): p. 1441-1446.

59. Han, X., et al. *The martensite structure and aging precipitates of a TiNiHf high temperature shape memory alloy*. in *Journal de Physique IV*. 1995.

60. Johnson, A., V. Martynov, and R. Minners. *Sputter deposition of high transition temperature Ti-Ni-Hf alloy thin films*. in *Journal de Physique IV*. 1995.

61. Mulder, J.H., *Investigation of High Temperature Shape Memory Alloys from the Ni-Ti-Zr and Ni-Ti-Hf Systems*. 1995, University of Twente.

62. Olier, P., et al. *Investigation of Transformation Temperatures Microstructure and Shape Memory Properties of NiTi, NiTiZr and NiTiHf Alloys*. in *Journal de Physique IV*. 1995.

63. Wu, K. and Z. Pu. *Martensite Transformation of (HfxTi50-x) Ni50Shape Memory Alloys*. in *Journal de Physique IV*. 1995.

64. Wu, K.H., et al. *The Shape Memory Effect of the NiTi-Hf High Temperature Shape Memory Alloy*. in *Shape Memory and Superelastic Technologies*. 1995. Pacific Grove California.

65. Han, X.D., et al., *Structure and substructure of martensite in a Ti36.5Ni48.5Hf15 high temperature shape memory alloy.* Acta Materialia, 1996. **44**(9): p. 3711-3721.

66. Wu, K., Z. Pu, and Y. Gao. *Study of NiTi-Hf and NiTi-Zr High-Temperature Shape Memory Alloys*. in *International Conference of Displacive Phase Transformations and their Applications in Materials Engineering*. 1996.

67. Zhang, C. and R.H. Zee. *Influence of thermo-mechanical processing of martensitic transformation of NiTi and NiTiHf shape memory alloys*. in *International Conference of Displacive Phase Transformations and their Applications in Materials Engineering*. 1996.

68. Gao, Y., Z. Pu, and K.H. Wu. *TEM Studies of NiTi-Hf and NiTi-Zr High-Temperature Shape Memory Alloys*. in *Shape Memory and Superelastic Technologies*. 1997. Pacific Grove California.

69. Golberg, D.V., et al., *Method of Manufacturing High-Temperature Shape Memory Alloys*. 1997. p. 1-12.

70. Han, X.D., et al., *Martensitic transformation in Ti36. 5Ni48. 5Hf15 high temperature shape memory alloy.* Materials Transactions, 1997. **38**(10): p. 842-851.

71. Han, X.D., et al., *In situ observations of the reverse martensitic transformations in a TiNiHf high temperature shape memory alloy.* Materials Letters, 1997. **30**(1): p. 23-28.

72. Potapov, P.L., et al., *Effect of Hf on the structure of Ni-Ti martensitic alloys.* Materials Letters, 1997. **32**(4): p. 247-250.

73. Shelyakov, A., et al. *Rapidly Quenched High Temperature Shape Memory NiTiHf Alloys*. in *Shape Memory and Superelastic Technologies*. 1997. Pacific Grove California.

74. Thoma, P.E., et al. *The Effect of Hafnium Content and Cycling under an Applied Axial Stress on the Creep and Martensite Strain of NiTi Based Shape Memory Alloy Wires* in *Journal de Physique IV* 1997.

75. Wang, Y., et al. *Microstructure and Mechnical Behavior of a Ni-Ti-Hf High Temperature Shape Memory Alloy*. in *Shape Memory and Superelastic Technologies*. 1997. Pacific Grove California.

76. Zhang, C., P.E. Thoma, and R.H. Zee. *The Influence of Hafnium Content, Cold Work, and Heat Treatment on the R-Phase Transformation of Niti Based Shape Memory Alloys*. in *Materials Research Society*. 1997. Cambridge University Press.

77. Gu, H.D., K.M. Leung, and C.Y. Chung, *Growth of high-temperature NiTi1−xHfxNiTi1−xHfx shape memory alloy thin films by laser ablation of composite targets.* Journal of Vacuum Science & Technology A, 1998. **16**: p. 3420-3422.

78. Gu, H.D., et al., *Growth of TiNiHf shape memory alloy thin films by laser ablation of composite targets.* Applied Surface Science, 1998. **127**: p. 579-583.

79. Han, X.D., et al., *A new precipitate phase in a TiNiHf high temperature shape memory alloy.* Acta Materialia, 1998. **46**(1): p. 273-281.

80. Zheng, Y.F., et al., *High-resolution electron microscopy study on the substructure of Ti–Ni–Hf B19′ Martensite.* Materials Letters, 1998. **36**(1): p. 142-147.

81. Zheng, Y.F., L.C. Zhao, and H.Q. Ye, *HREM Study on the Intervariant Structure of Ti-Ni-Hf B19′ Martensite.* Scripta Materialia, 1998. **38**(8): p. 1249-1253.

82. Besseghini, S., E. Villa, and A. Tuissi, *Ni-Ti-Hf shape memory alloy: effect of aging and thermal cycling.* Materials Science and Engineering: A, 1999. **273**: p. 390-394.

83. Cesari, E., et al., *Structure and properties of Ti–Ni–Zr and Ti–Ni–Hf melt-spun ribbons.* Materials Science and Engineering: A, 1999. **273-275**: p. 738-744.

84. Kang, S., H.-J. Im, and T.-H. Nam, *Effect of Hf-content on phase transformation behavior and microstructures of Ti-Ni-Hf shape memory alloys.* Journal of the Korean Institute of Metals and Materials(South Korea), 1999. **37**(11): p. 1281-1285.

85. Miyazaki, S. and A. Ishida, *Martensitic transformation and shape memory behavior in sputter-deposited TiNi-base thin films.* Materials Science and Engineering: A, 1999. **273**: p. 106-133.

86. Santamarta, R., et al., *Martensite stabilisation in Ni50Ti32.2Hf17.7.* Scripta Materialia, 1999. **41**(8): p. 867-872.

87. Thoma, P.E. and J.J. Boehm, *Effect of composition on the amount of second phase and transformation temperatures of NixTi90−xHf10 shape memory alloys.* Materials Science and Engineering: A, 1999. **273**: p. 385-389.

88. Wang, Y.Q., et al., *The tensile behavior of Ti36Ni49Hf15 high temperature shape memory alloy.* Scripta Materialia, 1999. **40**(12): p. 1327-1331.

89. Dalle, F., et al., *MeIt-spun ribbons of Ti-Hf-Ni-Re shape memory alloys: first investigations.* Scripta Materialia, 2000. **43**(4): p. 331-335.

90. Hsieh, S.F. and S.K. Wu, *Martensitic transformation of quaternary Ti50.5−XNi49.5ZrX/2HfX/2 (X=0–20 at.%) shape memory alloys.* Materials Characterization, 2000. **45**(2): p. 143-152.

91. Hsieh, S.F. and S.K. Wu, *Lattice parameters of martensite in Ti50.5−xNi49.5Zrx/2Hfx/2 quaternary shape memory alloys.* Journal of Alloys and Compounds, 2000. **312**(1): p. 288-294.

92. Liu, M., et al., *In situ TEM observations of martensite-austenite transformations in a Ni49Ti36Hf15 high temperature shape memory alloy.* Journal of Materials Science Letters, 2000. **19**(15): p. 1383-1386.

93. Meng, X.L., et al., *Effect of aging on the phase transformation and mechanical behavior of Ti36Ni49Hf15 high temperature shape memory alloy.* Scripta Materialia, 2000. **42**(4): p. 341-348.

94. Meng, X.L., et al., *Shape memory properties of the Ti36Ni49Hf15 high temperature shape memory alloy.* Materials Letters, 2000. **45**(2): p. 128-132.

95. Zhang, C., P.E. Thoma, and R. Zee. *High Hf content NiTiHf shape memory films*. in *Materials Research Society*. 2000.

96. Cesari, E., et al. *Ageing Effects in Ni-Ti Based Shape Memory Alloys*. in *Applied Crystallography: Proceedings of the XVIII Conference*. 2001. Wisla, Poland: World Scientific.

97. Dalle, F., et al., *MeIt-spun ribbons of Ti-Hf-Ni-Re shape memory alloys.* Scripta Materialia, 2001. **44**(6): p. 929-934.

98. Kang, S.-h. and T.-h. Nam, *Crystal structure of (TiHf)Ni phase formed in a 20Ti–50Ni–30Hf (at.%) alloy.* Metals and Materials International, 2001. **7**(5): p. 443-446.

99. Liang, X., et al., *Thermal cycling stability and two-way shape memory effect of Ni–Cu–Ti–Hf alloys.* Solid State Communications, 2001. **119**(6): p. 381-385.

100. Liu, M., et al., *Microstructure of melt-spinning high temperature shape memory Ni-Ti-Hf alloys.* Journal of Materials Science Letters, 2001. **20**(9): p. 827-830.

101. Meng, X.L., et al., *Microstructure of stress-induced martensite in a Ti–Ni–Hf high temperature shape memory alloy.* Scripta Materialia, 2001. **45**(10): p. 1177-1182.

102. Dalle, F., et al., *Interface mobility in Ni49.8Ti42.2Hf8 shape memory alloy.* Acta Materialia, 2002. **50**(14): p. 3557-3565.

103. Hsieh, S.F. and W.K. Chang, *Martensitic transformation of an aged/thermal-cycled Ti30.5Ni49.5Zr10Hf10 shape memory alloy.* Journal of Materials Science, 2002. **37**(14): p. 2851-2856.

104. Liu, L., et al. *Stress-Induced Martensitic Transformation and Microstructure of a Ti36Ni49Hf15 High-Temperature Shape-Memory Alloy*. in *Materials Science Forum*. 2002. Transtec Publications; 1999.

105. Meng, X.L., et al., *Stress-induced martensitic transformation behavior of a Ti–Ni–Hf high temperature shape memory alloy.* Materials Letters, 2002. **55**(1): p. 111-115.

106. Meng, X.L., et al., *Effect of Cu addition on phase transformation of Ti–Ni–Hf high-temperature shape memory alloys.* Materials Letters, 2002. **57**(2): p. 452-456.

107. Grummon, D.S., *Thin-film shape-memory materials for high-temperature applications.* Journal of Minerals, Metals and Materials Society, 2003. **55**(12): p. 24-32.

108. Jung, J., et al., *Precipitation of Heusler Phase (Ni 2 TiAl) from B2-TiNi in Ni-Ti-Al and Ni-Ti-Al-X (X= Hf, Zr) Alloys.* Metallurgical and Materials Transactions A, 2003. **34**(6): p. 1221-1235.

109. Jung, J., G. Ghosh, and G.B. Olson, *A comparative study of precipitation behavior of Heusler phase (Ni2TiAl) from B2-TiNi in Ni–Ti–Al and Ni–Ti–Al–X (X=Hf, Pd, Pt, Zr) alloys.* Acta Materialia, 2003. **51**(20): p. 6341-6357.

110. Manca, A., A.V. Shelyakov, and G. Airoldi, *Ageing in Parent Phase and Martensite Stabilization in a Ni50Ti30Hf20 Alloy.* Materials Transactions, 2003. **44**(6): p. 1219-1224.

111. Meng, X.L., et al., *Two-way shape memory effect induced by martensite deformation and stabilization of martensite in Ti36Ni49Hf15 high temperature shape memory alloy.* Materials Letters, 2003. **57**(26): p. 4206-4211.

112. Coluzzi, B., et al., *Damping spectrum of H-free and H-doped shape memory alloys NiTiHfCu at kHz frequencies.* Scripta Materialia, 2004. **51**(3): p. 199-202.

113. Firstov, G.S., J. Van Humbeeck, and Y.N. Koval, *Comparison of high temperature shape memory behaviour for ZrCu-based, Ti–Ni–Zr and Ti–Ni–Hf alloys.* Scripta Materialia, 2004. **50**(2): p. 243-248.

114. Firstov, G.S., J. Van Humbeeck, and Y.N. Koval, *High-temperature shape memory alloys.* Materials Science and Engineering: A, 2004. **378**(1): p. 2-10.

115. Meng, X.L., et al., *Two-way shape memory effect of a TiNiHf high temperature shape memory alloy.* Journal of Alloys and Compounds, 2004. **372**(1): p. 180-186.

116. Santamarta, R., et al., *Crystallization in partially amorphous Ni50Ti32Hf18 melt spun ribbon.* Materials Transactions, 2004. **45**(6): p. 1811-1818.

117. Santamarta, R., et al., *Thermal and microstructural evolution during the crystallization of a ni50Ti32Hf18 melt spun ribbon.* Archives of Metallurgy and Materials, 2004. **49**(4): p. 881-889.

118. Biscarini, A., et al., *Diffusion of hydrogen in the shape memory alloy Ni47Ti40Hf10Cu3.* Journal of Alloys and Compounds, 2005. **404**: p. 261-264.

119. Meng, X.L., et al., *Phase transformation and microstructure of quaternary TiNiHfCu high temperature shape memory alloys.* Intermetallics, 2005. **13**(2): p. 197-201.

120. Sanjabi, S., Y.Z. Cao, and Z.H. Barber, *Multi-target sputter deposition of Ni50Ti50–xHfx shape memory thin films for high temperature microactuator application.* Sensors and Actuators A: Physical, 2005. **121**(2): p. 543-548.

121. Tong, Y., et al., *Characterization of a nanocrystalline NiTiHf high temperature shape memory alloy thin film.* Scripta Materialia, 2005. **52**(10): p. 983-987.

122. Chastaing, K., et al., *Effect of Cu and Hf additions on NiTi martensitic transformation.* Materials Science and Engineering: A, 2006. **438**: p. 661-665.

123. Firstov, G., J. Van Humbeeck, and Y.N. Koval, *High temperature shape memory alloys problems and prospects.* Journal of Intelligent Material Systems and Structures, 2006. **17**(12): p. 1041-1047.

124. Kockar, B., et al., *A method to enhance cyclic reversibility of NiTiHf high temperature shape memory alloys.* Scripta Materialia, 2006. **54**(12): p. 2203-2208.

125. Meng, X.L., et al., *Effect of aging on martensitic transformation and microstructure in Ni-rich TiNiHf shape memory alloy.* Scripta Materialia, 2006. **54**(9): p. 1599-1604.

126. Meng, X.L., et al., *Phase transformation and precipitation in aged Ti–Ni–Hf high-temperature shape memory alloys.* Materials Science and Engineering: A, 2006. **438**: p. 666-670.

127. Sanjabi, S., S. Sadrnezhaad, and Z. Barber, *MEM5. 1 High Temperature NiTiHf Shape Memory Thin Films Fabricated by Simultaneous Sputter Deposition from Elemental Targets.* 2006.

128. Simon, A.A., *Shape memory response and microstructural evolution of a severe plastically deformed high temperature shape memory alloy (NiTiHf)*, in *Mechanical Engineering*. 2006, Texas A&M University. p. 81.

129. Wei, Q., X.D. Han, and Z. Zhang, *The substructures of martensite in a TiNiHf10 high temperature shape memory alloy.* Materials Letters, 2006. **60**(25): p. 3054-3058.

130. Zhang, Z., et al., *Vacuum induction melting of ternary NiTiX (X= Cu, Fe, Hf, Zr) shape memory alloys using graphite crucibles.* Materials Transactions, 2006. **47**(3): p. 661-669.

131. Ochin, P., et al., *Amorphous multielementary alloys: A preparation route for shape memory alloys.* Journal of Alloys and Compounds, 2007. **434**: p. 268-271.

132. Sanjabi, S., S. Sadrnezhaad, and Z. Barber, *Sputter alloying of Ni, Ti and Hf for fabrication of high temperature shape memory thin films.* Materials Science and Technology, 2007. **23**(8): p. 987-991.

133. Meng, X., et al. *Martensitic Transformation Behavior and Shape Memory Effect of an Aged Ni-rich Ti-Ni-Hf High Temperature Shape Memory Alloy*. in *Solid State Phenomena*. 2008. Trans Tech Publ.

134. Meng, X.L., et al., *Shape-memory behaviors in an aged Ni-rich TiNiHf high temperature shape-memory alloy.* Intermetallics, 2008. **16**(5): p. 698-705.

135. Muir Wood, A.J., et al., *Nanoindentation of binary and ternary Ni–Ti-based shape memory alloy thin films.* Surface and Coatings Technology, 2008. **202**(13): p. 3115-3120.

136. Resnina, N., S. Belyaev, and A. Shelyakov, *Martensitic transformation in amorphous-crystalline Ti-Ni-Cu and Ti-Hf-Ni-Cu thin ribbons.* The European Physical Journal-Special Topics, 2008. **158**(1): p. 21-26.

137. Tong, Y., Y. Liu, and J. Miao, *Phase transformation in NiTiHf shape memory alloy thin films.* Thin Solid Films, 2008. **516**(16): p. 5393-5396.

138. Zarinejad, M., Y. Liu, and T.J. White, *The crystal chemistry of martensite in NiTiHf shape memory alloys.* Intermetallics, 2008. **16**(7): p. 876-883.

139. Meng, X.L., et al., *Cu content and annealing temperature dependence of martensitic transformation of Ti36Ni49−xHf15Cux melt spun ribbons.* Intermetallics, 2009. **17**(12): p. 1078-1084.

140. Meng, X.L., et al., *Microstructure and martensitic transformation behaviors of a Ti–Ni–Hf–Cu high-temperature shape memory alloy ribbon.* Philosophical Magazine Letters, 2009. **89**(7): p. 431-438.

141. Resnina, N., S. Belyaev, and A. Shelyakov, *Influence of the dynamic crystallization conditions on the martensitic transformation in the Ti40. 7Hf9. 5Ni39. 8Cu10 shape memory alloy.* International Journal of Materials Research, 2009. **100**(3): p. 356-358.

142. Tong, Y., et al., *Microstructure and martensitic transformation of Ti49Ni51−xHfx high temperature shape memory alloys.* Materials Letters, 2009. **63**(21): p. 1869-1871.

143. Wojcik, C.C., *Properties and Heat Treatment of High Transition Temperature Ni-Ti-Hf Alloys.* Journal of Materials Engineering and Performance, 2009. **18**(5): p. 511-516.

144. Zarinejad, M., Y. Liu, and Y. Tong, *Transformation temperature changes due to second phase precipitation in NiTi-based shape memory alloys.* Intermetallics, 2009. **17**(11): p. 914-919.

145. Ded, G.S., *Characterization of Ni-rich NiTiHf based high temperature shape memory alloys*, in *Mechanical Engineering*. 2010. p. 233.

146. Ho, T.-J., S.-K. Wu, and K.-H. Lin, *Two-Stage Martensitic Transformation in Thermal-Cycled Ti40. 5Ni49. 5Hf10 Shape Memory Alloy.* Materials Transactions, 2010. **51**(4): p. 679-684.

147. Meng, X.L., et al., *Martensite structure in Ti–Ni–Hf–Cu quaternary alloy ribbons containing (Ti,Hf)2Ni precipitates.* Acta Materialia, 2010. **58**(10): p. 3751-3763.

148. Rao, J., et al., *Nickel titanium and nickel titanium hafnium shape memory alloy thin films.* Surface and Coatings Technology, 2010. **204**(15): p. 2331-2336.

149. Zarinejad, M. and Y. Liu, *Dependence of transformation temperatures of shape memory alloys on the number and concentration of valence electrons.* Shape Memory Alloys: Manufacture, Properties and Applications, 2010: p. 339.

150. Belyaev, S., N. Resnina, and V. Slesarenko, *Mechanical and functional properties of amorphous–crystalline thin ribbons of Ti 50 Ni 25 Cu 25 and Ti 40.7 Hf 9.5 Ni 44.8 Cu 5 shape memory alloys.* Smart Materials and Structures, 2011. **20**(8): p. 082003.

151. Belyaev, S., et al., *Mechanical and functional properties of amorphous-crystalline ribbons of Ti 40.7 Hf 9.5 Ni 44.8 Cu 5 alloy.* Inorganic Materials: Applied Research, 2011. **2**(5): p. 512-516.

152. Bigelow, G., et al., *NiTiHf High-Temperature Shape-Memory Alloys for near Term Applications.* Journal of Minerals, Metals and Materials Society, 2011.

153. Bigelow, G.S., et al., *Load-biased shape-memory and superelastic properties of a precipitation strengthened high-temperature Ni50.3Ti29.7Hf20 alloy.* Scripta Materialia, 2011. **64**(8): p. 725-728.

154. Coughlin, D., et al., *Stoichiometry and Aging Effects on the Microstructure and Properties of NiTiHf Shape Memory Alloys.* Journal of Minerals, Metals and Materials Society, 2011.

155. Denowh, C.M., *Thermomechanical training and characterization of Ni–Ti–Hf and Ni–Ti–Hf–Cu high temperature shape memory alloys*, in *Mechanical Engineering*. 2011. p. 118.

156. Karaca, H.E., et al., *Compressive response of nickel-rich NiTiHf high-temperature shape memory single crystals along the [111] orientation.* Scripta Materialia, 2011. **65**(7): p. 577-580.

157. Kim, H.Y., et al., *Cold workability and shape memory properties of novel Ti–Ni–Hf–Nb high-temperature shape memory alloys.* Scripta Materialia, 2011. **65**(9): p. 846-849.

158. König, D., et al., *Phase transformation, structural and functional fatigue properties of Ti–Ni–Hf shape memory thin films.* Acta Materialia, 2011. **59**(8): p. 3267-3275.

159. Moshref-Javadi, M., et al., *Effect of Aging on the Microstructure and Shape Memory Effect of a Hot-Rolled NiTiHf Alloy.* Journal of Materials Engineering and Performance, 2011. **20**(4): p. 618-622.

160. Moshref-Javadi, M., et al., *Heat Treatment of a (Ti, Hf)-Rich NiTiHf High Temperature Shape Memory Alloy.* 2011.

161. Motemani, Y., et al., *Analysis of Ti–Ni–Hf shape memory alloys by combinatorial nanocalorimetry.* Acta Materialia, 2011. **59**(20): p. 7602-7614.

162. Wang, B., et al., *Production of Ni-35Ti-15Hf alloy via the FFC Cambridge process.* Journal of The Electrochemical Society, 2011. **158**(10): p. D595-D602.

163. Belbasi, M., M.T. Salehi, and S.A.A.A. Mousavi, *Hot Deformation Behavior of NiTiHf Shape Memory Alloy Under Hot Compression Test.* Journal of Materials Engineering and Performance, 2012. **21**(12): p. 2594-2599.

164. Benafan, O., *Deformation and phase transformation processes in polycrystalline NiTi and NiTiHf high temperature shape memory alloys*, in *Mechanical, Materials and Aerospace Engineering*. 2012, University of Central Florida. p. 259.

165. Benafan, O., et al., *Microstructural Response During Isothermal and Isobaric Loading of a Precipitation-Strengthened Ni-29.7Ti-20Hf High-Temperature Shape Memory Alloy.* Metallurgical and Materials Transactions A, 2012. **43**(12): p. 4539-4552.

166. Coughlin, D., et al. *Characterization of Nickel Rich NiTiHf Shape Memory Alloys for Use as High Temperature Actuators*. in *AIP Conference Proceedings*. 2012. American Institute of Physics, Ste. 1 NO 1 Melville NY 11747-4502 United States.

167. Coughlin, D.R., et al., *Characterization of the microstructure and mechanical properties of a 50.3Ni–29.7Ti–20Hf shape memory alloy.* Scripta Materialia, 2012. **67**(1): p. 112-115.

168. Denowh, C.M. and D.A. Miller, *Thermomechanical training and characterization of Ni–Ti–Hf and Ni–Ti–Hf–Cu high temperature shape memory alloys.* Smart Materials and Structures, 2012. **21**(6): p. 065020.

169. Evirgen, A., et al., *Effect of aging on the martensitic transformation characteristics of a Ni-rich NiTiHf high temperature shape memory alloy.* Functional Materials Letters, 2012. **5**(04): p. 1250038.

170. Karaca, H.E., et al., *Effects of aging on [111] oriented NiTiHfPd single crystals under compression.* Scripta Materialia, 2012. **67**(7): p. 728-731.

171. Karaca, H.E., et al., *Superelastic response and damping capacity of ultrahigh-strength [111]-oriented NiTiHfPd single crystals.* Scripta Materialia, 2012. **67**(5): p. 447-450.

172. Mosca, H.O., G. Bozzolo, and M.F. del Grosso, *Atomistic modeling of ternary additions to NiTi and quaternary additions to Ni–Ti–Pd, Ni–Ti–Pt and Ni–Ti–Hf shape memory alloys.* Physica B: Condensed Matter, 2012. **407**(16): p. 3244-3247.

173. Van Humbeeck, J., *Shape memory alloys with high transformation temperatures.* Materials Research Bulletin, 2012. **47**(10): p. 2966-2968.

174. Xiaoyun, S., L. Yan, and L. Shusuo, *Effect of Hf Addition on the High-Temperature Deformation Behavior of Ni-Ti-Al Alloys.* Rare Metal Materials and Engineering, 2012. **10**: p. 010.

175. Yang, F., et al., *High Resolution Microscopy Analysis of a New Precipitate Phase in Ni-rich NiTiHf and NiPdTiHf High Temperature Shape Memory Alloys.* Microscopy and Microanalysis, 2012. **18**(S2): p. 366.

176. Acar, E., et al., *Role of aging time on the microstructure and shape memory properties of NiTiHfPd single crystals.* Materials Science and Engineering: A, 2013. **573**: p. 161-165.

177. Acar, E., et al., *Characterization of the shape memory properties of a Ni45.3Ti39.7Hf10Pd5 alloy.* Journal of Alloys and Compounds, 2013. **578**: p. 297-302.

178. Belbasi, M., et al., *A study on the mechanical behavior and microstructure of NiTiHf shape memory alloy under hot deformation.* Materials Science and Engineering: A, 2013. **560**: p. 96-102.

179. Belbasi, M., M.T. Salehi, and S.H. Seyedin, *Hot tensile property and fracture behavior of as-cast Ni49Ti36Hf15 shape memory alloy produced by vacuum induction melting.* Materials & Design, 2013. **49**: p. 981-985.

180. Coughlin, D.R., *Characterization of Stoichiometric and Aging Effects on NiTiHf High Temperature Shape Memory Alloys*, in *Materials Science and Engineering*. 2013, The Ohio State University. p. 174.

181. Karaca, H., et al., *Shape memory behavior of high strength NiTiHfPd polycrystalline alloys.* Acta Materialia, 2013. **61**(13): p. 5036-5049.

182. Karaca, H.E., et al., *Effects of nanoprecipitation on the shape memory and material properties of an Ni-rich NiTiHf high temperature shape memory alloy.* Acta Materialia, 2013. **61**(19): p. 7422-7431.

183. Moshref-Javadi, M., et al., *Age-induced multi-stage transformation in a Ni-rich NiTiHf alloy.* Acta Materialia, 2013. **61**(7): p. 2583-2594.

184. Santamarta, R., et al., *TEM study of structural and microstructural characteristics of a precipitate phase in Ni-rich Ni–Ti–Hf and Ni–Ti–Zr shape memory alloys.* Acta Materialia, 2013. **61**(16): p. 6191-6206.

185. Shukla, D., R.D. Noebe, and P. Stebner Aaron, *Empirical Study of the Multiaxial, Thermomechanical Behavior of NiTiHf Shape Memory Alloys*. 2013. p. 1-52.

186. Suresh, K.S., et al., *Evolution of microstructure and texture in Ni49.4Ti38.6Hf12 shape memory alloy during hot rolling.* Intermetallics, 2013. **42**: p. 1-8.

187. Yang, F., et al., *Structure analysis of a precipitate phase in an Ni-rich high-temperature NiTiHf shape memory alloy.* Acta Materialia, 2013. **61**(9): p. 3335-3346.

188. Yang, F., et al., *Composition Analysis on the Precipitates in the NiTiHf and NiPdTiHf Alloys.* Microscopy and Microanalysis, 2013. **19**(S2): p. 1518-1519.

189. Acar, E., *Precipitation, orientation and composition effects on the shape memory properties of high strength NiTiHfPd alloys*, in *Mechanical Engineering*. 2014, University of Kentucky. p. 230.

190. Acar, E., et al., *Orientation dependence of the shape memory properties in aged Ni45.3Ti29.7Hf20Pd5 single crystals.* Intermetallics, 2014. **54**: p. 60-68.

191. Azeem, M.A. and D. Dye, *In situ evaluation of the transformation behaviour of NiTi-based high temperature shape memory alloys.* Intermetallics, 2014. **46**: p. 222-230.

192. Belbasi, M. and M.T. Salehi, *Influence of Chemical Composition and Melting Process on Hot Rolling of NiTiHf Shape Memory Alloy.* Journal of Materials Engineering and Performance, 2014. **23**(7): p. 2368-2372.

193. Benafan, O., et al., *Mechanical and functional behavior of a Ni-rich Ni50.3Ti29.7Hf20 high temperature shape memory alloy.* Intermetallics, 2014. **50**: p. 94-107.

194. Evirgen, A., *Microstructural Characterization and Shape Memory Response of Ni-Rich NiTiHf and NiTiZr High Temperature Shape Memory Alloys*, in *Materials Science and Engineering*. 2014. p. 256.

195. Hornbuckle, B.C., *Investigations in phase stability and mechanical attributes in nickel-rich Nitinol with and without hafnium additions*, in *Metallurgical Engineering*. 2014, The University of Alabama. p. 143.

196. Jo, J.-W., et al., *Effect of Ni Content on the Aging Behavior of Ti-xNi-12Hf (x= 50.2 ~ 51.0)(at%) Alloys.* Science of Advanced Materials, 2014. **6**(9): p. 2015-2019.

197. Karaca, H., et al., *NiTiHf-based shape memory alloys.* Materials Science and Technology, 2014. **30**(13): p. 1530-1544.

198. Kim, J.H., et al., *Effects of Microstructure and Deformation Conditions on the Hot Formability of Ni–Ti–Hf Shape Memory Alloys.* Journal of Nanoscience and Nanotechnology, 2014. **14**(12): p. 9548-9553.

199. Kim, K.M., et al., *High temperature oxidation behavior of Ti–Ni–Hf shape memory alloy.* Thermochimica Acta, 2014. **583**: p. 1-7.

200. Moshref-Javadi, M., et al., *Fabrication of (Ti,Hf)-rich NiTiHf Alloy Using Graphitic Mold and Crucible.* Journal of Materials Science and Technology, 2014. **30**(3): p. 280-284.

201. Prasher, M. and D. Sen, *Influence of aging on phase transformation and microstructure of Ni50.3Ti29.7Hf20 high temperature shape memory alloy.* Journal of Alloys and Compounds, 2014. **615**: p. 469-474.

202. Prasher, M., et al. *Small angle x-ray scattering study of nano-scale precipitation in Ni 50.3 Ti 29.7 Hf 20 high temperature shape memory alloy*. in *AIP Conference Proceedings*. 2014. AIP.

203. Stebner, A., et al. *Unique deformation mechanisms of an ultra-high strength NiTiHf alloy*. 2014.

204. Stebner, A.P., et al., *Transformation strains and temperatures of a nickel–titanium–hafnium high temperature shape memory alloy.* Acta Materialia, 2014. **76**: p. 40-53.

205. Suresh, K.S., et al., *Evolution and stability of phases in a high temperature shape memory alloy Ni49.4Ti38.6Hf12.* Intermetallics, 2014. **44**: p. 18-25.

206. Wang, J. and H. Sehitoglu, *Modelling of martensite slip and twinning in NiTiHf shape memory alloys.* Philosophical Magazine, 2014. **94**(20): p. 2297-2317.

207. Acar, E., *Dynamic mechanical response of a Ni45.7Ti29.3Hf20Pd5 alloy.* Materials Science and Engineering: A, 2015. **633**: p. 169-175.

208. Acar, E., E.O. Osman, and E.K. Haluk, *Experimental investigation and modeling of the loading rate and temperature dependent superelastic response of a high performance shape-memory alloy.* Smart Materials and Structures, 2015. **24**(7): p. 075020.

209. Acar, E., et al., *Compressive response of Ni45.3Ti34.7Hf15Pd5 and Ni45.3Ti29.7Hf20Pd5 shape-memory alloys.* Journal of Materials Science, 2015. **50**(4): p. 1924-1934.

210. Atli, K., et al., *Work production using the two-way shape memory effect in NiTi and a Ni-rich NiTiHf high-temperature shape memory alloy.* Smart Materials and Structures, 2015. **24**(12): p. 125023.

211. Belyaev, S., N. Resnina, and A. Shelyakov, *Pseudoelasticity effect in amorphous—crystalline Ti 40.7 Hf 9.5 Ni 44.8 Cu 5 shape memory alloy.* Smart Materials and Structures, 2015. **24**(4): p. 045013.

212. Benafan, O., et al., *On the Recovery Stress of a Ni50. 3Ti29. 7Hf20 High Temperature Shape Memory Alloy*. 2015.

213. Carl, M., et al. *Effect of Heat Treating on Precipitate Phases in NiTiHf*. in *ASME 2915 Conference on Smart Materials, Adaptive Structures and Intelligent Systems*. 2015. American Society of Mechanical Engineers.

214. Casalena, L., et al., *Transformation and deformation characterization of NiTiHf and NiTiAu high temperature shape memory alloys.* Microscopy and Microanalysis, 2015. **21**: p. 607-608.

215. Coppa, A.C., et al., *Influence of Dilute Hf Additions on Precipitation and Martensitic Transformation in Ni-Ti-Pd Alloys.* Journal of Minerals, Metals and Materials Society, 2015. **67**(10): p. 2244-2250.

216. Evirgen, A., et al., *Microstructural characterization and shape memory characteristics of the Ni50.3Ti34.7Hf15 shape memory alloy.* Acta Materialia, 2015. **83**: p. 48-60.

217. Hornbuckle, B.C., R.D. Noebe, and G.B. Thompson, *Influence of Hf solute additions on the precipitation and hardenability in Ni-rich NiTi alloys.* Journal of Alloys and Compounds, 2015. **640**: p. 449-454.

218. Hornbuckle, B.C., et al., *Structure–property relationships in a precipitation strengthened Ni–29.7Ti–20Hf (at%) shape memory alloy.* Materials Science and Engineering: A, 2015. **637**: p. 63-69.

219. Hsu, D.H.D., et al., *The effect of aluminum additions on the thermal, microstructural, and mechanical behavior of NiTiHf shape memory alloys.* Journal of Alloys and Compounds, 2015. **638**: p. 67-76.

220. Karaca, H.E., et al., *Microstructure and transformation related behaviors of a Ni45.3Ti29.7Hf20Cu5 high temperature shape memory alloy.* Materials Science and Engineering: A, 2015. **627**: p. 82-94.

221. Li, P., H.E. Karaca, and Y.-T. Cheng, *Spherical indentation of NiTi-based shape memory alloys.* Journal of Alloys and Compounds, 2015. **651**: p. 724-730.

222. McCluskey, P.J., et al., *Application of in-situ nano-scanning calorimetry and X-ray diffraction to characterize Ni–Ti–Hf high-temperature shape memory alloys.* Thermochimica Acta, 2015. **603**: p. 53-62.

223. Owusu-Danquah, J.S., et al., *A Comparative Study of Ni49.9Ti50.1 and Ni50.3Ti29.7Hf20 Tube Actuators.* Journal of Materials Engineering and Performance, 2015. **24**(4): p. 1726-1740.

224. Panchenko, E.Y., et al., *Superelasticity in high-strength heterophase single crystals of Ni51. 0Ti36. 5Hf12. 5 alloy.* Technical Physics Letters, 2015. **41**(8): p. 797-800.

225. Patriarca, L. and H. Sehitoglu, *High-temperature superelasticity of Ni50.6Ti24.4Hf25.0 shape memory alloy.* Scripta Materialia, 2015. **101**: p. 12-15.

226. Resnina, N., et al., *Pre-martensitic phenomena in Ti40.7Hf9.5Ni44.8Cu5 shape memory alloy.* Intermetallics, 2015. **67**: p. 69-74.

227. Resnina, N., et al., *Influence of crystalline phase volume fraction on the two-way shape memory effect in amorphous–crystalline Ti40.7Hf9.5Ni44.8Cu5 alloy.* Materials Science and Engineering: A, 2015. **627**: p. 65-71.

228. Saghaian, S.M., *Shape memory behavior of single crystal and polycrystalline Ni-rich NiTiHf high temperature shape memory alloys*, in *Mechanical Engineering*. 2015, University of Kentucky. p. 198.

229. Saghaian, S.M., et al., *Effects of aging on the shape memory behavior of Ni-rich Ni50.3Ti29.7Hf20 single crystals.* Acta Materialia, 2015. **87**: p. 128-141.

230. Santamarta, R., et al., *Effect of Thermal Treatments on Ni–Mn–Ga and Ni-Rich Ni–Ti–Hf/Zr High-Temperature Shape Memory Alloys.* Shape Memory and Superelasticity, 2015. **1**(4): p. 418-428.

231. Surikov, N.Y., et al. *Stress-induced martensitic transformation in high-strength [236]-oriented Ni 51 Ti 36.5 Hf 12.5 single crystals*. in *IOP Conference Series: Materials Science and Engineering*. 2015.

232. Tagiltsev, A., et al. *Stress-Induced Thermoelastic Martensitic Transformations and Functional Properties in [011]-oriented NiTiHfPd Single Crystals*. in *IOP Conference Series: Materials Science and Engineering*. 2015. IOP Publishing.

233. Wu, Y., et al., *Shape memory response of polycrystalline NiTi12. 5Hf alloy: transformation at small scales.* Shape Memory and Superelasticity, 2015. **1**(3): p. 387-397.

234. Acar, E., et al., *Microstructure and shape memory behavior of [111]-oriented NiTiHfPd alloys.* Smart Materials and Structures, 2016. **25**(3): p. 035011.

235. Benafan, O., et al., *Constant-Strain Thermal Cycling of a Ni50.3Ti29.7Hf20 High-Temperature Shape Memory Alloy.* Shape Memory and Superelasticity, 2016. **2**(2): p. 218-227.

236. Bucsek, A.N., et al., *Composition, Compatibility, and the Functional Performances of Ternary NiTiX High-Temperature Shape Memory Alloys.* Shape Memory and Superelasticity, 2016. **2**(1): p. 62-79.

237. Casalena, L., et al., *Revealing Transformation and Deformation Mechanisms in NiTiHf and NiTiAu High Temperature Shape Memory Alloys Through Microstructural Investigations.* Microscopy and Microanalysis, 2016. **22**(3): p. 1954-1955.

238. Coughlin, D., et al., *Microstructure–property relationships in a high-strength 51Ni–29Ti–20Hf shape memory alloy.* Journal of Materials Science, 2016. **51**(2): p. 766-778.

239. Evirgen, A., et al., *Relationship between crystallographic compatibility and thermal hysteresis in Ni-rich NiTiHf and NiTiZr high temperature shape memory alloys.* Acta Materialia, 2016. **121**: p. 374-383.

240. Kim, J.H., et al., *Effect of yttrium on martensite-austenite phase transformation temperatures and high temperature oxidation kinetics of Ti-Ni-Hf high-temperature shape memory alloys.* Metals and Materials International, 2016. **22**(2): p. 204.

241. Kim, K.M., et al., *Comparative Study of the Thermocyclic Behavior of Ti–Ni–Hf and Ti–Ni–Hf–Ta Shape Memory Alloys.* Journal of Nanoscience and Nanotechnology, 2016. **16**(11): p. 11775-11778.

242. Kim, S.-W., et al., *Fracture toughness of TiNiHf alloys: A hybrid study using in-situ transmission electron microscopy experiments and finite element analyses.* Materials Science and Engineering: A, 2016. **655**: p. 363-372.

243. Kornegay, S.M., *Influence of zirconium additions on nitinol shape memory phase stability, transformation temperatures, and thermo-mechanical properties*, in *Metallurgical and Materials Engineering*. 2016, The University of Alabama. p. 163.

244. Manuel, M.V., *Nickel titanium alloys, methods of manufacture thereof and article comprising the same*. 2016, Google Patents. p. 1-3.

245. Panchenko, E.Y., et al., *Orientation Dependence of Functional Properties in Heterophase Single Crystals of the Ti36. 5Ni51. 0Hf12. 5 and Ti48. 5Ni51. 5 Alloys.* Russian Physics Journal, 2016. **58**(11): p. 1534-1543.

246. Patriarca, L., et al., *High-temperature functional behavior of single crystal Ni51.2Ti23.4Hf25.4 shape memory alloy.* Acta Materialia, 2016. **106**: p. 333-343.

247. Patriarca, L., et al., *High temperature shape memory behavior of Ni50.3Ti25Hf24.7 single crystals.* Scripta Materialia, 2016. **115**: p. 133-136.

248. Pushin, V.G., et al., *Structure and thermoelastic martensitic transformations in ternary Ni–Ti–Hf alloys with a high-temperature shape memory effect.* Technical Physics, 2016. **61**(7): p. 1009-1014.

249. Pushin, V.G., et al., *Structural and phase transformations, mechanical properties, and shape-memory effects in quasibinary Ni50Ti38Hf12 alloy obtained by quenching from the melt.* Physics of Metals and Metallography, 2016. **117**(12): p. 1251-1260.

250. Pushin, V.G., et al., *Thermoelastic martensitic transformations, mechanical properties, and shape-memory effects in rapidly quenched Ni45Ti32Hf18Cu5 alloy in the ultrafine-grained state.* Physics of Metals and Metallography, 2016. **117**(12): p. 1261-1269.

251. Resnina, N., S. Belyaev, and A. Shelyakov, *Isothermal B2→B19′ martensitic transformation in Ti40.7Hf9.5Ni44.8Cu5 shape memory alloy.* Scripta Materialia, 2016. **112**: p. 106-108.

252. Saghaian, S., et al., *Effects of Ni content on the shape memory properties and microstructure of Ni-rich NiTi-20Hf alloys.* Smart Materials and Structures, 2016. **25**(9): p. 095029.

253. Saghaian, S.M., et al., *Tensile shape memory behavior of Ni50.3Ti29.7Hf20 high temperature shape memory alloys.* Materials & Design, 2016. **101**: p. 340-345.

254. Stanford, M.K., *Hardness and Microstructure of Binary and Ternary Nitinol Compounds*. 2016. p. 1-46.

255. Timofeeva, E.E., et al., *Effects of ageing on microstructure and superelastic behavior of [110]-oriented Ni45.3Ti29.7Hf20Pd5 single crystals.* Materials Science and Engineering: A, 2016. **674**: p. 498-503.

256. Wu, Y., et al., *Ultrahigh tensile transformation strains in new Ni50.5Ti36.2Hf13.3 shape memory alloy.* Scripta Materialia, 2016. **118**: p. 51-54.

257. Young, S., et al., *Diffusion Pack Cementation of Hf Powders on Ni–Ti Shape Memory Alloys.* Science of Advanced Materials, 2016. **8**(10): p. 1923-1926.

258. Zhao, C. and X. Meng, *Microstructure evolution and phase transformation in thermally cycled Ni–Ti–Hf film.* Modern Physics Letters B, 2016. **30**(20): p. 1650263.

259. Abuzaid, W. and H. Sehitoglu, *Functional fatigue of Ni50.3Ti25Hf24.7 – Heterogeneities and evolution of local transformation strains.* Materials Science and Engineering: A, 2017. **696**: p. 482-492.

260. Benafan, O. and J.G. Darrell, *High temperature shape memory alloy Ni50.3Ti29.7Hf20 torque tube actuators.* Smart Materials and Structures, 2017. **26**(9): p. 1-14.

261. Canadinc, D., et al., *On the deformation response and cyclic stability of Ni50Ti35Hf15 high temperature shape memory alloy wires.* Scripta Materialia, 2017. **135**: p. 92-96.

262. Elahinia, M., et al., *Additive Manufacturing of NiTiHf High Temperature Shape Memory Alloy*. 2017. p. 1-16.

263. Hong, S.H., et al., *Influence of Zr content on phase formation, transition and mechanical behavior of Ni-Ti-Hf-Zr high temperature shape memory alloys.* Journal of Alloys and Compounds, 2017. **692**: p. 77-85.

264. Joy, J.K., et al. *Predicting the constitutive response of precipitation hardened NiTiHf*. in *International Society for Optical Engineering*. 2017. International Society for Optics and Photonics.

265. Karakoc, O., et al., *Effects of upper cycle temperature on the actuation fatigue response of NiTiHf high temperature shape memory alloys.* Acta Materialia, 2017. **138**: p. 185-197.

266. Kim, J.H. and S. Young, *Effect of Yttrium on Microstructural Evolution and High Temperature Compressive Behavior of Ti–Ni–Hf High Temperature Shape Memory Alloys.* Science of Advanced Materials, 2017. **9**(6): p. 1028-1031.

267. Liu, J.L., et al., *Investigation of the phase equilibria in Ti-Ni-Hf system using diffusion triples and equilibrated alloys.* Calphad, 2017. **58**: p. 160-168.

268. Owusu-Danquah, J.S. and A.F. Saleeb, *On the modeling of the effect of processing and heat treatment on actuation behaviors of high temperature ternary and quaternary shape memory alloys.* Journal of Alloys and Compounds, 2017. **714**: p. 493-501.

269. Panchenko, E., et al. *Stress-ageing effects on the functional properties of high-strength [001]-oriented Ni51.0Ti37.3Hf12.5 single crystals*. in *Materials Today*. 2017.

270. Prasad, R.V.S., et al., *Microstructure and phase transformation behavior of a new high temperature NiTiHf-Ta shape memory alloy with excellent formability.* Journal of Alloys and Compounds, 2017. **697**: p. 55-61.

271. Resnina, N., et al., *Violation of the sequence of martensite crystals formation on cooling and their shrinking on heating during B2↔ B19′ martensitic transformation in Ti40. 7Hf9. 5Ni44. 8Cu5 shape-memory alloy.* Phase Transitions, 2017. **90**(3): p. 289-298.

272. Saghaian, S.M., et al., *High strength NiTiHf shape memory alloys with tailorable properties.* Acta Materialia, 2017. **134**: p. 211-220.

273. Sehitoglu, H., L. Patriarca, and Y. Wu, *Shape memory strains and temperatures in the extreme.* Current Opinion in Solid State and Materials Science, 2017. **21**(2): p. 113-120.

274. Sehitoglu, H., Y. Wu, and L. Patriarca, *Shape memory functionality under multi-cycles in NiTiHf.* Scripta Materialia, 2017. **129**: p. 11-15.

275. Sehitoglu, H., et al., *Superelasticity and Shape Memory Behavior of NiTiHf Alloys.* Shape Memory and Superelasticity, 2017. **3**(2): p. 168-187.

276. Stanford, M.K., *Hardness and Second Phase Percentage of Ni-Ti-Hf Compounds After Heat Treatment at 700C*. 2017. p. 1-24.

277. Tagiltsev, A., et al. *Tension-compression asymmetry in Ni45.3Ti29.7Hf20Pd5 single crystals*. in *Materials Today*. 2017.

278. Wheeler III, R.W., *Actuation Fatigue Characterization Methods and Lifetime Predictions of Shape Memory Alloy Actuators*, in *Aerospace Engineering*. 2017. p. 221.

279. Wu, Y., E. Ertekin, and H. Sehitoglu, *Elastocaloric cooling capacity of shape memory alloys – Role of deformation temperatures, mechanical cycling, stress hysteresis and inhomogeneity of transformation.* Acta Materialia, 2017. **135**: p. 158-176.

280. Yi, X., et al., *Martensitic transformation behaviors and mechanical properties of (Ti 36 Ni 49 Hf 15) 100-x Y x high temperature shape memory alloys.* Journal of Alloys and Compounds, 2017. **705**: p. 98-104.

281. Carl, M., B. Van Doren, and M.L. Young, *In Situ Synchrotron Radiation X-ray Diffraction Study on Phase and Oxide Growth during a High Temperature Cycle of a NiTi-20 at.% Zr High Temperature Shape Memory Alloy.* Shape Memory and Superelasticity: p. 1-12.

282. Javadi, M.M., et al., *Effect of aging on the microstructure and shape memory effect of a hot-rolled NiTiHf alloy.* Journal of materials engineering and performance, 2011. **20**(4-5): p. 618-622.

283. Ley, N.A., O. Benafan, and M.L. Young, *Characterization of Thermo-Mechanically Processed High Temperature NiTiHf20 Shape Memory Wires.* 2018.

284. International, A., *Standard Test Method for Energy Dispersive X-Ray Spectrometer (EDX) Analysis of Metallic Surface Condition for Gas Distribution System Components*. 2016, ASTM International: West Conshohocken, PA.

285. International, A., *Standard Test Method for Transformation Temperature of Nickel-Titanium Alloys by Thermal Analysis*. 2016, ASTM International: West Conshohocken, PA.

286. International, A., *Standard Test Methods for Vickers Hardness and Knoop Hardness of Metallic Materials*. 2016, ASTM International: West Conshohocken, PA.

287. Khalil-Allafi, J., A. Dlouhy, and G. Eggeler, *Ni 4 Ti 3-precipitation during aging of NiTi shape memory alloys and its influence on martensitic phase transformations.* Acta Materialia, 2002. **50**(17): p. 4255-4274.

288. Michutta, J., et al., *Martensitic phase transformation in Ni-rich NiTi single crystals with one family of Ni 4 Ti 3 precipitates.* Materials Science and Engineering: A, 2004. **378**(1): p. 152-156.

289. Amini, A. and C. Cheng, *Nature of hardness evolution in nanocrystalline NiTi shape memory alloys during solid-state phase transition.* Scientific reports, 2013. **3**: p. 2476.